THE JOURNAL OF BIOLOGICAL CHEMISTRY VOL. 290, NO. 34, pp. 21114–21130, August 21, 2015

Dimethylated H3K27 Is a Repressive Epigenetic Histone Mark in the Protist *Entamoeba histolytica* and Is Significantly Enriched in Genes Silenced via the RNAi Pathway*

Received for publication, March 4, 2015, and in revised form, June 23, 2015 Published, JBC Papers in Press, July 6, 2015, DOI 10.1074/jbc.M115.647263

Bardees M. Foda[‡§] **and Upinder Singh**[‡¶1]

From the Departments of [‡]*Internal Medicine, Division of Infectious Diseases, and* [¶]*Microbiology and Immunology, School of Medicine, Stanford University, Stanford, California 94305 and the* [§]*Department of Molecular Genetics and Enzymology, National Research Centre, Dokki, Egypt*

Background: *Entamoeba histolytica* has an RNAi-mediated TGS pathway but the epigenetic marks are not known.
Results: H3K27Me2 is an inducible repressive histone modification enriched in loci silenced by small RNAs.
Conclusion: Transcriptional gene silencing and chromatin modification are coupled to maintain prolonged gene silencing.
Significance: This work identifies the first repressive histone mark in *Entamoeba* and links it to RNAi.

RNA interference (RNAi) is a fundamental biological process that plays a crucial role in regulation of gene expression in many organisms. Transcriptional gene silencing (TGS) is one of the important nuclear roles of RNAi. Our previous data show that *Entamoeba histolytica* has a robust RNAi pathway that links to TGS via Argonaute 2-2 (Ago2-2) associated 27-nucleotide small RNAs with 5′-polyphosphate termini. Here, we report the first repressive histone mark to be identified in *E. histolytica*, dimethylation of H3K27 (H3K27Me2), and demonstrate that it is enriched at genes that are silenced by RNAi-mediated TGS. An RNAi-silencing trigger can induce H3K27Me2 deposits at both episomal and chromosomal loci, mediating gene silencing. Our data support two phases of RNAi-mediated TGS: an active silencing phase where the RNAi trigger is present and both H3K27Me2 and Ago2-2 concurrently enrich at chromosomal loci; and an established silencing phase in which the RNAi trigger is removed, but gene silencing with H3K27Me2 enrichment persist independently of Ago2-2 deposition. Importantly, some genes display resistance to chromosomal silencing despite induction of functional small RNAs. In those situations, the RNAi-triggering plasmid that is maintained episomally gets partially silenced and has H3K27Me2 enrichment, but the chromosomal copy displays no repressive histone enrichment. Our data are consistent with a model in which H3K27Me2 is a repressive histone modification, which is strongly associated with transcriptional repression. This is the first example of an epigenetic histone modification that functions to mediate RNAi-mediated TGS in the deep-branching eukaryote *E. histolytica*.

Regulation of gene expression is central to multiple biological processes including differentiation, development, and tumorigenesis (1–3). Specifically, maintenance of a silenced state is vital in several situations; for example, silencing specific genes in humans can prevent diseases such as parasitic infections, cancer, or developmental dysregulation resulting in embryonic death (4–6). One method by which silencing is affected is by alteration of the chromatin state via post-translational modifications of the N-terminal tails of histones, which converts the chromatin from an active to a repressed state. Covalent modifications of histone tails provide binding sites for chromatin-binding proteins, which control the condensation levels of chromatin and the functional activity of the underlying genetic elements. Thus, assembly of highly condensed chromatin (*i.e.* heterochromatin) at certain loci hinders transcription (7). Methylation of histones has been shown to be an important modification for heterochromatin formation and propagation. In fungi, plants, fission yeast, and animals, methylation of lysine 9 of histone H3 (H3K9Me)[2] is crucial for heterochromatin assembly (6, 8, 9). Additionally, other methylated histones including H3K27Me, H3K36Me, and H4K20Me have been implicated in gene silencing in diverse situations including worm development and germline X chromosome silencing (10–16). Moreover, TGS mediated by DNA methylation has been noted in plants and the fruit fly (17, 18).

RNAi is a means of regulating gene expression in many biological systems ranging from protozoans to humans (19–22). The initiation of RNAi is via small RNA molecules whose sequence information identifies genes to be targeted for silencing. The machinery that ultimately mediates gene silencing is the RNA-induced silencing complex, containing the catalytically active Argonaute (Ago) proteins. Other important proteins for RNAi include Dicer (an RNase III enzyme that generates small RNAs) and RNA-dependent RNA polymerase (RdRP), which amplifies small RNAs in some systems (23). The RNAi pathway can mediate gene silencing through transcriptional gene silencing (TGS) or through post-translational gene

* This work was supported, in whole or in part, by National Institutes of Health Grants R01AI053724 and R21 AI102277 (to U. S.). The authors declare that they have no conflicts of interest with the contents of this article.
[1] To whom correspondence should be addressed. Tel.: 650-723-4045; Fax: 650-724-3892; E-mail: usingh@stanford.edu.

[2] The abbreviations used are: H3K27Me2, dimethylated histone H3 lysine 27; sRNA, small RNA; Eh, *Entamoeba histolytica*; *RdRP*, RNA-dependent RNA polymerase; *Ago2-2*, Argonaute 2-2; RPL21, ribosomal protein L21; *Ap-A*, amoebapore A; *ROM*, rhomboid protease; Pol II, RNA polymerase II; TGS, transcriptional gene silencing.

silencing (P-TGS) by RNA degradation or translational repression (24, 25). RNAi-mediated TGS is facilitated by a complex of small RNAs bound to an RNA-induced transcriptional silencing complex. RNA-induced transcriptional silencing targets homologous DNA sequences where it induces recruitment of chromatin modifying factors and heterochromatin formation that result in silencing of target genes. The extensive interdependence between the RNAi machinery and heterochromatin assembly has been illustrated in *Saccharomyces pombe, Tetrahymena thermophila, Drosophila melanogaster, Caenorhabditis elegans,* and animals (26–31). In animals and fission yeast, fulfillment of both the siRNA pathway and repressive histone depositions are required for assembly of heterochromatin at appropriate genetic regions to achieve transcriptional repression (32).

Entamoeba histolytica is a protozoan parasite and an important human pathogen. Despite its position as a deep-branching eukaryote, *E. histolytica* has a distinct and complex endogenous RNAi pathway mediated by 27-nucleotide 5′-poly-P small RNAs that map antisense to genes and mediate TGS via a nuclear-localized Argonaute protein (33, 34). We have recently developed a robust silencing tool in ameba by harnessing the endogenous RNAi pathway. With this approach, a gene with abundant antisense small RNAs can "trigger" silencing of a new gene fused to it through the generation of small RNAs to the fused gene (35). We were able to demonstrate stable gene repression, including ongoing silencing despite loss of the trigger construct hinting that the long term stable down-regulation may be mediated by epigenetic memory. Although many genes could be silenced using this approach, we also identified some genes that could not be silenced despite the generation of functional small RNAs (36). It has previously been demonstrated that RNAi-silenced loci have increased histone occupancy, however, given the sequence divergence of the amebic H3, commercially available reagents could not be applied to define the molecular modifications typically associated with heterochromatin (33, 37).

In the present study, we shed light on mechanisms of RNAi-regulated TGS in *E. histolytica*. We identified an amebic histone modification, dimethylated lysine 27 histone H3 (H3K27Me2), and generated and validated reagents for its characterization. Using custom antibodies to H3K27, H3K27Me2, and Argonaute 2-2 for chromatin immunoprecipitation (ChIP) followed by PCR analysis, we identified that the H3K27Me2 modification, along with the amebic Argonaute 2-2 protein, marks genes that are undergoing active RNAi-based gene silencing. Furthermore, we demonstrated that the H3K27Me2 modification is subsequently enriched to mediate stable long term RNAi-based silencing; however, long term stable silencing is no longer marked by Argonaute deposition. This work is the first to identify a specific histone repressive mark, H3K27Me2, in the deep branching protist, *E. histolytica*, and provides the first molecular link between the amebic RNAi pathway and heterochromatin-mediated transcriptional gene silencing. Furthermore, to our knowledge methylated H3K27 has not previously been recognized in parasite systems, thus adding to the novelty of the observation for the parasitology field.

Experimental Procedures

Antibody Generation—Rabbit polyclonal antibodies against two forms of *E. histolytica* histone H3 were custom generated by 21st Century Biochemicals, Marlboro, MA. Affinity purified antibodies were obtained by immunizing rabbits with H3K27 synthetic peptide (Ahx-VAFKAA(K)KMLSKD) for generating anti-H3K27 and H3K27Me2 peptide (Ahx-VAFKAA(KMe2)KMLSKD) for generating anti-H3K27Me2 (Fig. 1*A*). The percentage of dimethylated Lys-27 in H3K27Me2 peptide preparations was 99%. Anti-EhAgo2-2 and anti-EhRBP9 (or anti-Pol II) antibodies were generated in previous studies (33, 38). Commercial antibodies included a pan-specific mouse anti-actin antibody (MP Biomedicals, Burlingame, CA); secondary HRP-conjugated anti-mouse and anti-rabbit antibodies (Jackson ImmunoResearch, West Grove, PA) were also utilized.

Peptide Competition Assays and Western Blot Analysis—Increasing amounts (50, 100, 200, 500, and 1000 ng) of synthetic peptides H3K27, H3K27Me2, and an irrelevant peptide (RNase III (Ac-RSSLEKYQTD)) were blotted directly on a nitrocellulose membrane (Bio-Rad). The membrane was left to dry and then blocked with 5% milk in 1× Tris-buffered saline/Tween 20 (TBS-T) for 1 h. To block α-H3K27 or α-H3K27Me2 antibodies, increasing amounts of each peptide were used for blocking fixed amounts of the antibodies. We incubated 1 μg of H3K27 or H3K27Me2 antibody with increasing amounts of each peptide (10, 25, 50, or 100 μg). The mixtures was completed to 100 μl of 1× TBS-T and kept on a gentle rotator at room temperature for 2 h. To remove possible aggregates and avoid subsequent Western blot background, the peptide/antibody mixture was centrifuged for 15 min at 14,000 rpm at 4 °C. Next, we incubated each supernatant (*i.e.* blocked antibody), 1 μg of unblocked antibody, or preimmune serum with the peptides blotted on the membranes overnight then proceeded with the Western blot protocol. To test antibody specificity against *E. histolytica* histone H3, as in the peptide competition assays described above, we blocked the antibody with different peptide amounts (2, 4, 10, 20, 50, and 100 μg). Blocked or unblocked antibodies or preimmune serum were used to probe increasing amounts of whole cell lysates (10, 20, 40, and 80 μg).

Parasite Culture and Transgenic Strains—*E. histolytica* trophozoites (HM-1:IMSS) were grown according to standard conditions (39, 40). *E. histolytica* strains containing trigger silencing or Myc overexpression constructs were previously generated (34, 35). Briefly, the 19-Trigger strains, 19T-ROM1, 19T-Ago2-2, and 19T-RdRP1, contain a silencing construct that has a short Trigger region fused to the full-length *EhROM1*, *EhAgo2-2*, or *EhRdRP1*, respectively. Similarly, overexpression parasite lines, Myc-ROM1, Myc-Ago2-2, and Myc-RdRP1, contain constructs with N-terminal 3× Myc tag preceding a full-length *EhROM1*, *EhAgo2-2*, or *EhRdRP1* coding region, respectively. Both the silencing and overexpression constructs were built using the pKT plasmid as a backbone, which contains the 5′ and 3′ regulatory regions of the cysteine synthase gene; thus all generated constructs including the Trigger-silencing constructs were driven by the same cysteine synthase promoter (41). We maintained the cell lines at 12 μg/ml of

G418 for EhAgo2-2 and EhRdRP and 6 μg/ml of G418 for EhROM1. A cell line, 19T-ROM1$^{\text{No plasmid}}$, was generated by maintaining 19T-ROM1 trophozoites in TYI-S-33 medium without the G418 selection marker for greater than 2 years and loss of Trigger plasmid was confirmed by drug susceptibility and PCR (35).

Immunofluorescence Microscopy—Fluorescence microscopy was performed as described previously (33). Wild type *E. histolytica* trophozoites were grown for 48 h. Confluent cells were allowed to adhere onto a glass slide chamber (Thermo Fisher) for 3 h at 37 °C in TYI-S-33 medium. Cells were rinsed once with 1× PBS and fixed for 30 s with methanol/acetone (50:50) at room temperature. The cells were rinsed once with 1× PBS, permeabilized by 250 μl of PBS containing 0.1% Triton X-100 for 10 min at 37 °C, washed 3 times with 1× PBS, followed by blocking in 3% BSA-PBS for 1 h at room temperature. Blocked cells were incubated overnight at 4 °C with 1% BSA/PBS containing 1:100-diluted rabbit polyclonal H3K27Me2 antibody with gentle agitation. Following four washes with 1× PBS for 10 min each, the cells were incubated in the dark with 1% BSA/PBS containing a 1:200 dilution of fluorescent secondary antibody, anti-rabbit Alexa 488 (Cell Signaling) for 1 h at room temperature. After staining, cells were washed in 1× PBS four times each for 10 min with gentle shaking in the dark. Cells were mounted with 25 μl of Vectashield mounting medium with DAPI (Vector Laboratories) and visualized using a Leica CTR6000 microscope, using a Becton Dickinson CARVII confocal unit. Images were analyzed using Leica LAS-AF software.

RNA Isolation and RT-PCR—Total RNA was extracted from multiple independent biological replicates of *E. histolytica* trophozoites including wild type (HM-1:IMSS), 19T-ROM1$^{\text{No plasmid}}$, 19T-ROM1, 19T-Ago2-2, 19T-RdRP1, Myc-ROM1, Myc-Ago2-2, and Myc-RdRP1. Trophozoites were grown for 48 h and RNA was collected using a miRVANA kit (Ambion) according to the manufacturer's instructions. RNA was treated with a DNA-free DNase kit (Invitrogen) to remove any residual DNA, and reverse transcribed using oligo(dT) primer and a reverse transcription kit (Invitrogen). DNA templates served as positive controls and were prepared by either isolating DNA from cell lines using the RNeasy Plant Mini Kit (Qiagen) or by plasmid DNA purification. Primers for RT-PCR were designed as follow: *EHI_048600*, 5′-TGCAAATGATTTAGGAGGAACA and 3′-GAGGGTTGTTGAGAATGAAGTTG; *EHI_199600*, 5′-ACGTCATGCTGAATTTGCTG and 3′-CCTTTAAGCCCAGCCTTTCT. For all episomal genes: 5′-ACACCCGGGATGTCTTCAGCTCAACCAA; episomal *EhROM1*, 3′-TTAAAATAATTCACAGGAATTGGCA; episomal *EhAgo2-2*, 3′-GCTTCTGGAACTGAAACCATTCTACCA; episomal *EhRdRP1*, 3′-ATGAGTTGTTCCTTGTTTACTATT; EhRdRP1, 5′-CATTCTCATGCACCTGCAAC and 3′-TTCGAGCAAATGGAATCACA; *EhAgo2-2*, 5′-ATTAGAGACATGGACCAACCATTACTTG and 3′-ACGATCATAGAAATTAGCAAGTTGATG; *EhROM1*, 5′-TGAACACTTTAGGAGCGAAGAA and 3′-GCAAGACATATAATTGGGCAAA; *EhAp-A*, 5′-GGATGAAAGCCATCGTCTTTGT and 3′-CCCTTCAATAAGTTGGATGAGTT; Myc, 5′-TCTAGAATGGAACAAAAACTTATTTCAG.

Chromatin Immunoprecipitation Assays—ChIP protocol was modified from the method described by Abcam and adapted for the *E. histolytica* specific antibodies. *E. histolytica* cell lines (HM-1:IMSS, 19T-ROM1, 19T-ROM1$^{\text{No plasmid}}$, 19T-Ago2-2, 19T-RdRP1, Myc-ROM1, Myc-Ago2-2, and Myc-RdRP1) were grown axenically at 37 °C in TYI-S-33 medium. Trophozoites (2×10^7) were grown at confluence and cross-linked with 1% formaldehyde for 10 min at 37 °C. Glycine (to a final concentration of 0.125 M) was added for 5 min at 37 °C to stop the cross-linking. Adherent cells were washed twice in PBS, chilled, and pelleted by spinning for 5 min at 4 °C. Pelleted cells were suspended in 1 ml of ChIP cell lysis buffer (20 mM Tris-HCl, pH 8, 85 mM KCl, 0.5% Nonidet P-40, protease inhibitor mixtures) and incubated on ice for 10 min. The nuclei were isolated by spinning the cell lysate for 5 min at 1000 rpm. Isolated nuclei were incubated on ice for 10 min with nuclear lysis buffer (50 mM Tris-HCl, pH 8, 10 mM EDTA, 1.0% SDS, protease inhibitor mixtures). Chromatin was sonicated to an average length of 500 bp and centrifuged to remove residual insoluble materials. Supernatant was pre-cleared with 80 μl of protein-A agarose/salmon sperm slurry beads (EMD Millipore) for 30 min at 4 °C. Cleared lysate was diluted 5-fold in ChIP dilution buffer (0.01% SDS, 1.1% Triton X-100, 1.1 EDTA, 20 mM Tris-HCl, pH 8.0, 167 mM NaCl). A supernatant volume representing 10% of total soluble chromatin was put aside at 20 °C as input for subsequent steps. Diluted lysate (equivalent to 2×10^6 cells) was incubated with each antibody overnight at 4 °C on a gentle rotator. Polyclonal antibodies used in ChIP experiments included 5 μg of each *E. histolytica* anti-H3K27 and anti-H3K27Me2 antibodies (both customized by 21st Century Biochemicals), anti-EhAgo2-2 (customized by EZBiolab), anti-RPB9 (38), and IgG as a control (Cell Signaling). Following antibody incubation, 80 μl of protein A-agarose/salmon sperm slurry beads were added and incubated for 3 h at 4 °C. The beads were washed consecutively for 3 min on a rotator two times with low salt wash buffer (0.1% SDS, 1% Triton X-100, 2 mM EDTA, 20 mM Tris-HCl, pH 8.0, 150 mM NaCl), twice with high salt wash buffer (0.1% SDS, 1% Triton X-100, 2 mM EDTA, 20 mM Tris-HCl, pH 8.0, 500 mM NaCl), one time with LiCl wash buffer (0.25 M LiCl, 1% Nonidet P-40, 1% Na-deoxycholate, 1 mM EDTA, 20 mM Tris-HCl, pH 8.0), and two times with TE buffer (10 mM Tris-HCl, pH 8.0, 1 mM EDTA). Protein-DNA complex was eluted from protein-A or protein-G beads used with anti-RPB9 antibody by adding two times 250 μl of elution buffer (1% SDS, 2 mM EDTA, 50 mM Tris-HCl, pH 8.0) and incubating each for 15 min at 65 °C each time and vortexing every 5 min; 500 μl of eluate was subsequently collected. Protein-DNA cross-linking was reversed by adding NaCl to a final concentration of 200 mM and heating at 65 °C overnight. RNase treatment was performed using 20 μg of RNase A (Sigma) at 37 °C for 1 h followed by treatment with 128 μl of Proteinase K mixture (160 μg of Proteinase K, 625 mM Tris-HCl, pH 6.5, 156.25 mM EDTA) for 2 h at 45 °C. DNA was extracted using 500 μl of phenol/chloroform/isoamyl alcohol (Invitrogen), and enriched DNA was collected after 5 min of spinning at room temperature at 14,000 rpm. Collected DNA was cleaned by a PCR purification kit according to the manufacturer's instructions (Qiagen) and eluted with 50 μl of DNase-free water.

ChIP-PCR Analysis—PCR (total volume 25 μl) were run using 4 μl of ChIP-eluted enriched DNA and 1 unit of platinum *Taq* DNA polymerase (Invitrogen) to amplify a DNA fragment of 100–200 bp size. To amplify only the episomal DNA fragment, forward primers were designed to specifically anneal to the episomal promoter (cysteine synthase), Myc tag, or the 19-Trigger; the reverse primer was specific to the gene of interest. For identifying the chromosomal region of a target gene, the forward primers were designed to anneal specifically to the endogenous promoter of the target gene and the reverse primers were the same as used for amplifying the episomal fragments. The coding region primers anneal to the coding region of the target gene, in both the episomal and chromosomal copies, given that they have an identical sequence. The number of PCR cycles was set to 30 for amplifying the episomal or coding fragments and 35 for amplifying the chromosomal regions. PCR products were analyzed on a 1.5% agarose gel and results were analyzed using the Quantity One software (Bio-Rad) to measure the band intensity. The enrichment was calculated as percentage of the input and compared with the steady state level of enrichment at the gene encoding ribosomal protein L21 (*RPL21*), a constitutively expressed gene. To calculate fold-enrichment, the data were normalized to that of *RPL21* and subsequently the normalized average values were compared with a control cell line. The levels of enrichment are represented as the mean ± S.E. of a minimum of 3 independent ChIP experiments. ChIP-PCR primers designed as following: *EHI_048600*, 5′-ACACCCGGGATGGAAATTGAATTAACCC and 3′-ACACCTAGGCGTTGATGCTGCAATTTTT; *EhAp-A*, 5′-AAACAATCATGAAAGCCATCG and 3′-GCTTTATTGCAAAGGCTGC; *EhRPL21* (coding region), 5′-CTAACGGTAGAAATAGAAGAACCAG and 3′-TCCAAACACGTCCAGTCTTTC; *EhRPL21* (promoter region), TAATAAACTAGTAACTTGAACCCTTGCTGGTTCTTCTATTTCTACCGTTAG; episomal promoter, 5′-CGTAAAAAAGTTATTGTTGCATCTATT. *EHI_197520*: for 19-Trigger plasmids, 3′-CGTGGTAGTTGGTTGAGCTGAAGACAT; Myc, for Myc-overexpression plasmids, 3′-GGTAAGTTTTTGTTCGCTAGCCAT; *EhROM1* (coding region), 5′-AGGCCTCATTCTCCACCACATAACAATA and 3′-TTAATCATCATCCATATCTTTGTAAACA; *EhAgo2-2* (coding region): 5′-GGTACCATGCAACCATCAATTCACGATT and 3′-TTTTTGGAAGAGAGGCATAAAAATC; *EhRdRP1* (coding region), 5′-CCCGGGATGGATAAATTTGATTATTGTC and 3′-GGCAATATCTCCAATAAAATCAAGGCA; *EhROM1* (chromosomal promoter region), 5′-GGTAAGAAGAGAAAATGAAAATAAAAA and 3′-GGTCATTACTCCAATCAAATGTATGTA; *EhAgo2-2* (chromosomal promoter region), 5′-CCGATCTAATTTAGCCAATTATAT and 3′-GGTTTATCAATTGTTTGGTCATTTGAG; Episomal *EhRdRP1* (chromosomal promoter region), 5′-GGTAAACCAAATAAAAAAAAAACAAAA and 3′-GGCAATATCTCCAATAAAATCAAGGCA.

Results

Generation of E. histolytica Histone α-H3K27 and α-H3K27Me2 Antibodies—E. histolytica histone H3 has a highly divergent N terminus (Fig. 1*A*) (42). However, conserved lysine residues, which are targets for post-translational modifications, are maintained in the *E. histolytica* histone H3 tail. In higher eukaryotes, enrichment of methylated H3K27 is associated with gene repression (13, 14, 43, 44). Hence, we asked whether coupling of H3K27 methylation and transcriptional gene silencing is conserved in *E. histolytica*. We synthesized peptides to represent unmodified H3 (H3K27) and a dimethylated form of H3 (H3K27Me2) (H3K27Me2 peptide preparation had 99% dimethylated Lys-27), and generated rabbit polyclonal antibodies against each. Each antibody recognizes a single band at the expected molecular mass of 15 kDa using Western blot analysis (Fig. 1*B*). Reactivity of H3K27Me2 antibody strongly suggests the presence of a methylated form of lysine 27 in *E. histolytica* H3.

To determine the affinity of the α-H3K27 and the α-H3K27Me2 antibodies, we immobilized increasing amounts of H3K27 and H3K27Me2 peptides on a nitrocellulose membrane and incubated it with anti-H3K27 or anti-H3K27Me2 antibody. Each antibody displayed a very strong affinity toward the peptide used for antibody generation (Fig. 1, *C* and *D*), whereas the preimmune serum did not (data not shown). Neither antibody reacted with the RNase III peptide, which served as an irrelevant peptide control (data not shown). To verify specificity of the antibodies, peptide competition assays were conducted in which we blocked each antibody with H3K27, H3K27Me2, or RNase III peptide (Fig. 1, *C* and *D*). We used increasing amounts of the peptides to block a fixed quantity of each antibody and then used the blocked antibody to probe different amounts of immobilized peptides. At antibody:peptide ratios of 1:10 and 1:25 μg, we noticed that the affinity of α-H3K27/H3K27- or α-H3K27Me2/H3K27Me2-blocked antibody decreased significantly. In contrast, both antibodies retained strong affinity when we used the same ratios to block the antibodies with nonspecific peptides (*i.e.* H3K27Me2 and RNase III peptides to block α-H3K27, or H3K27 and RNase III peptides for blocking α-H3K27Me2). Similar results were obtained when we increased the amount of blocking peptides to 50 or 100 μg (data not shown). Despite the specificity, each antibody showed some reactivity toward both peptide forms, H3K27 and H3K27Me2, which we attribute to the substantial similarity in peptide sequences. We extended the specificity test and probed increasing amounts of whole cell lysate with α-H3K27 or α-H3K27Me2 antibody each blocked with H3K27, H3K27Me2, and RNase III peptides (Fig. 1, *E* and *F*). Similar to results from the peptide competition assays, when we blocked either α-H3K27 or α-H3K27Me2 antibody with the cognate peptide, the Western blot signal was greatly reduced. In contrast, we observed strong immunodetection for α-H3K27 and α-H3K27Me2 antibodies when we blocked them with an irrelevant peptide. These results demonstrate that α-H3K27 and α-H3K27Me2 antibodies bind with greater specificity to *E. histolytica* H3K27 and H3K27Me2 histone forms, respectively.

Dimethylation of Lysine 27 of Histone H3 Is a Repressive Epigenetic Mark in E. histolytica—Cross-talk between RNAi and H3K27 methylation leads to gene repression through heterochromatin condensation in multiple systems (14, 43). To determine whether H3K27Me2 associates with the condensed chromatin in *E. histolytica*, we performed immunofluorescence analysis. The tendency of heterochromatin to be visualized as

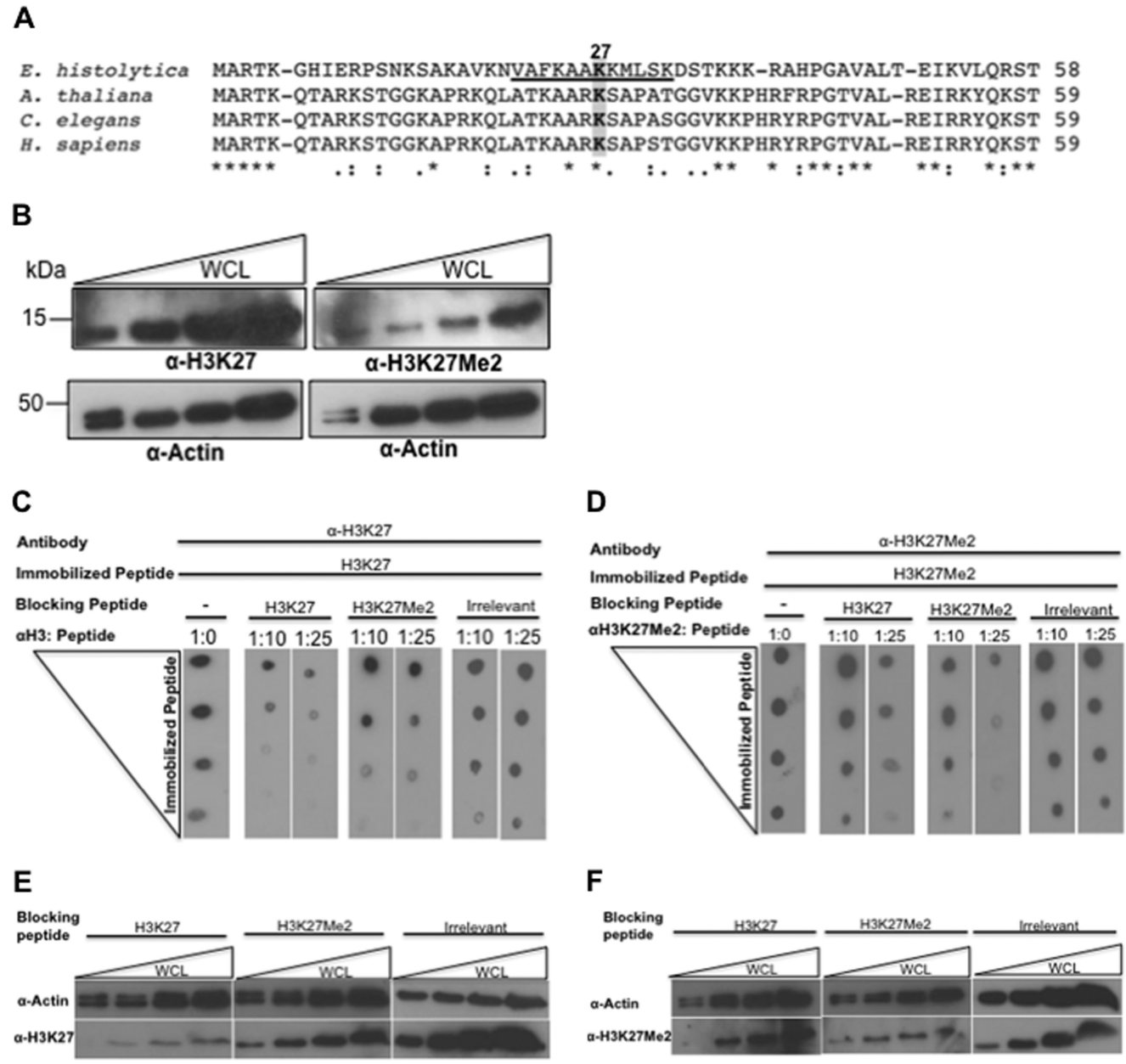

FIGURE 1. ***E. histolytica* H3 may be methylated on lysine 27.** *A,* sequence analysis of N terminus of *E. histolytica* histone H3 aligned using ClustalW with homologous H3 sequence from different organisms. *Shaded bold lysine residue*: a highly conserved lysine, K27. *Underlined amino acids*: used for peptide synthesis. *: identical amino acids; a *colon* indicates conserved amino acids; a *period* indicates semi-conserved amino acids. *B,* Western blot analysis for increasing amounts of whole cell lysate (*WCL*) prepared from wild type *E. histolytica* trophozoites. Total protein resolved by SDS-PAGE then transferred to PVDF membrane and analyzed for *E. histolytica* H3K27, dimethylated H3K27 (H3K27Me2), or actin. *C–F*, both generated *E. histolytica* α-H3K27 and α-H3K27Me2 antibodies have high specificity. *C,* peptide competition assays. Increasing amounts of H3K27 peptide were immobilized on dot-blot nitrocellulose membrane. The membranes were probed with α-H3K27 antibody alone or α-H3K27 antibody blocked as indicated with different amounts of H3K27, H3K27Me2, or irrelevant (RNase III) peptide. *D,* same as *C* but the immobilized peptides are H3K27Me2 and membranes were probed with unblocked or blocked α-H3K27Me2 antibody in the same way as in *C*. *E,* Western blot analysis of increasing amounts of whole cell lysate from wild type trophozoites. Total protein was probed with unblocked α-H3K27 antibody or α-H3K27 antibodies blocked with 20 ng of each H3K27, H3K27Me2, or irrelevant (RNase III) peptide. Actin is used as a loading control. *F*, same as *E*, however, the probing antibody is the unblocked or blocked α-H3K27Me2 antibody as in *E*.

discrete foci is attributed to its condensed nature (45, 46). We stained wild type *E. histolytica* cells with H3K27Me2 antibody and identified discrete foci in the parasite nucleus, which co-localized with DAPI staining and that most likely represent the heterochromatin (Fig. 2*A*).

Previously, using a commercial α-H3 antibody we and others have demonstrated increased occupancy of H3 at loci affected by small RNA (sRNA)-mediated gene silencing in the *E. histolytica* G3 strain (33, 37). To more specifically investigate the mechanism of small RNA-induced transcriptional gene silencing, we asked if post-translationally modified H3 histone (H3K27Me2) contributes to small RNA gene silencing in *E. histolytica*. To answer this question, we performed ChIP assays to establish the correlation between small RNAs, gene silencing, and histone modifications in *E. histolytica*. To determine whether H3K27Me2 is enriched at silenced loci with abundant antisense small RNAs, we selected an amebic gene, *EHI_048600*, which has numerous antisense sRNAs and is

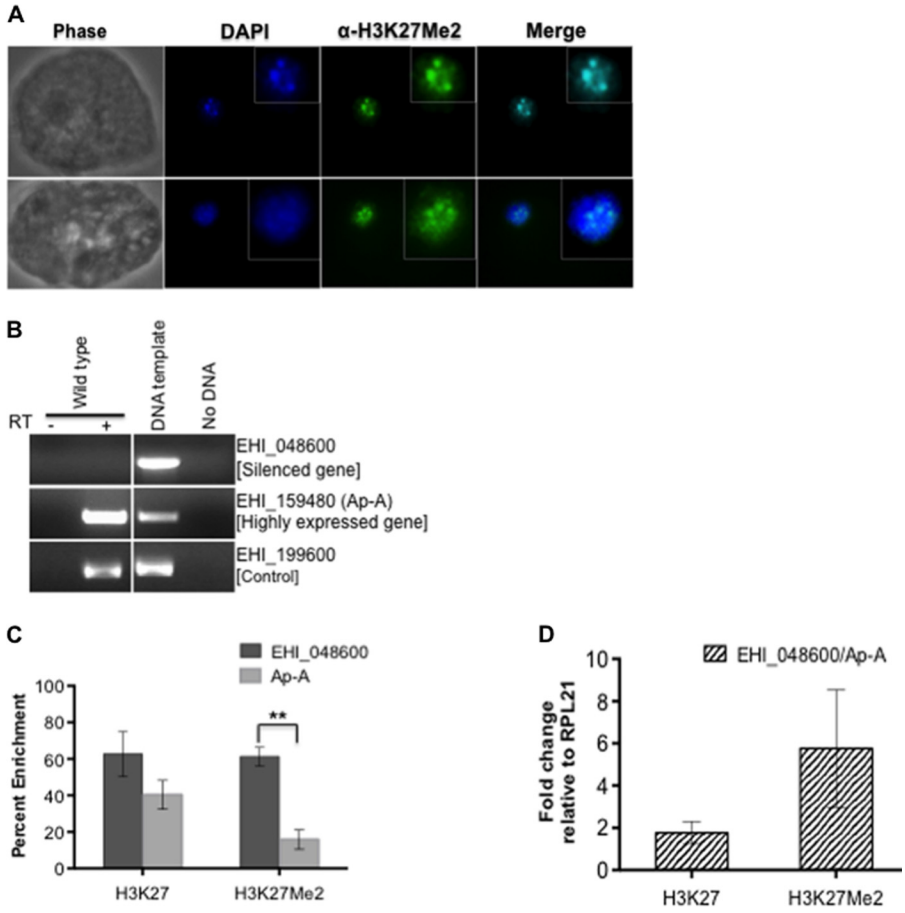

FIGURE 2. **H3K27Me2 is associated with heterochromatin and significantly enriched at endogenously silenced loci in *E. histolytica*.** *A,* immunofluorescence analysis of wild type *E. histolytica* cells using anti-H3K27Me2 antibody. Anti-H3K27Me2 stains nuclear foci, which co-localize with DAPI densely stained DNA domains. About 100-slice planes of confocal images were analyzed on *Z*-axis. Shown are three-dimensional images for single slices. *B,* RT-PCR analysis of RNA collected from wild type *E. histolytica* trophozoites. Very low expression of *EHI_048600* and high transcript levels of *Ap-A* are noted compared with the constitutively expressed *EHI_199600* gene. DNA template is genomic DNA prepared from wild type cells. *C,* endogenously silenced *EHI_048600* gene is significantly enriched with H3K27Me2. ChIP-PCR analysis of wild type trophozoites treated with formaldehyde and nuclear extract immunoprecipitated with control IgG or antibodies specific for *E. histolytica* proteins H3K27 or H3K27Me2. Percent enrichment represents levels of endogenously silenced *EHI_048600* or highly expressed *Ap-A* enriched with *E. histolytica* H3K27 or H3K27Me2. Enrichment was calculated as a percentage of enriched coding regions after subtracting IgG background and relative to input DNA. Enrichment levels at the constitutively expressed *RPL21* gene was calculated in the same manner. *D,* increase in *RPL21* normalized levels of *EHI_048600* enriched with repressive H3K27Me2 as compared with *Ap-A*-enriched regions. The chart displays the ratio of enrichment values at the *EHI_048600* coding region normalized to *RPL21* relative to that at Ap-A (also normalized to *RPL21*). Data represent mean ± S.E. of at least three independent ChIP experiments. *, $p < 0.05$; **, $p < 0.01$; ***, $p < 0.001$.

silenced (35). Additionally, we included a highly expressed gene Amoebapore A (*Ap-A*) as a negative control. RT-PCR experiments highlight the different expression levels of the selected genes (very low expression of *EHI_048600* and high levels of *Ap-A*) (Fig. 2*B*). To determine whether H3K27Me2 is enriched at silenced genes, we performed ChIP assays followed by PCR analysis to evaluate the abundance of H3K27Me2 at genes with distinct expression levels. Relative to the input DNA, we identified statistically significant enrichment of H3K27Me2 at the silenced gene (*EHI_048600*) compared with very low levels of H3K27Me2 at the highly expressed *Ap-A* gene (61.2% ± 5.1 compared with 15.7 ± 5.3%; $p = 0.003$) (Fig. 2*C*). To calculate the difference in enrichment between the two genes, we measured the levels of enrichment at a constitutively expressed gene, *RPL21*, and used it for normalization. We detected a 6-fold increase of *EHI_048600* enriched with H3K27Me2 as compared with enriched DNA of *Ap-A* (Fig. 2*D*). The H3K27 antibody showed no significant enrichment at *EHI_048600* (1.7-fold ± 2.7; $p = 0.2$), which agrees with the previous results of the commercial H3 antibody. Overall, these data imply that the majority of histone depositions at the silenced locus are H3K27Me2. These results indicate that H3K27Me2 is a repressive epigenetic mark in *E. histolytica* and may be responsible for maintaining transcriptional gene silencing.

RNAi-silenced ROM1 Gene Has Enriched Repressive Histone H3K27Me2 Deposition—Our laboratory has recently established a method for trigger-induced sRNA-mediated gene silencing in *E. histolytica*, which induces gene down-regulation by generating pools of antisense small RNAs to the target gene (35). In this manner, multiple genes including Rhomboid protease 1 (*ROM1*), Myb-transcription factor, and an H_2O_2-responsive transcription factor were down-regulated (47). These genes also displayed long term silencing despite removal of the trigger plasmid. However, other amebic genes such as Argonaute genes (*EhAgo2-1*, *EhAgo2-2*, and *EhAgo2-3*) and EhRNase III were resistant to gene silencing using the trigger approach, despite generation of abundant and functional small RNAs to these genes (36). The RNA-dependent RNA polymer-

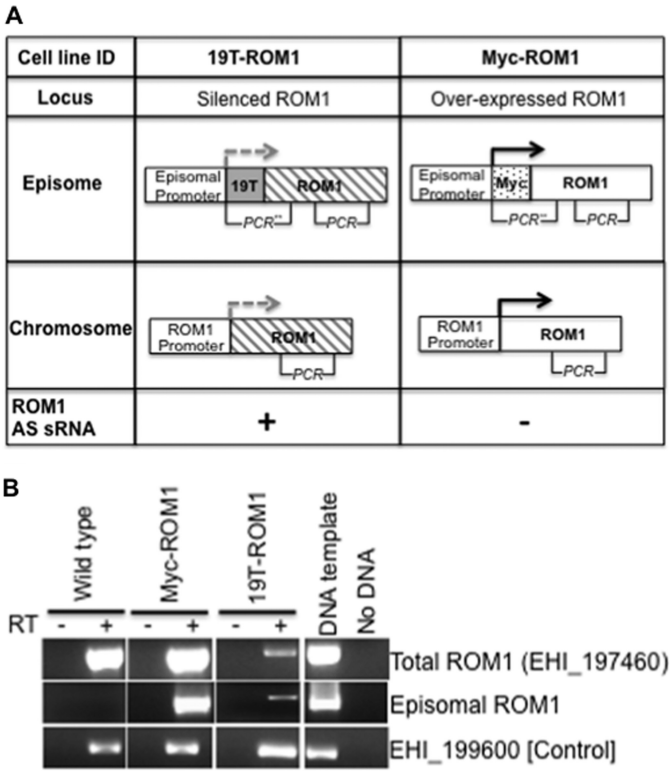

FIGURE 3. **Silencing trigger is able to reduce gene expression of both episomal and chromosomal *ROM1* loci.** *A,* schematic diagram for 19 trigger-ROM1 (*19T-ROM1*) silencing construct and Myc-ROM1 overexpression plasmid (Myc-ROM1). The two constructs have the same vector backbone and are driven by the same promoter and regulatory sequences. *ROM1* antisense sRNAs are present in 19T-ROM1. *Striped box*, silent gene; *PCR,* amplified regions displayed in *B*; **, episomal specific region. *B,* RT-PCR analysis of RNA collected from 19T-ROM1 and Myc-ROM1 *E. histolytica* trophozoites. As diagramed in *A*, PCR primers were used to represent total levels of *ROM1* transcribed from both *ROM1* loci (episomal and chromosomal). Levels of episomal *ROM1* transcript evaluated by primers designed specifically to amplify episomal transcript. Expression levels of the *EHI_199600* gene serve as a reference control. *DNA template,* genomic DNA or plasmid DNA (for episomal *ROM1*, only PCR product of 19T-ROM1 is shown).

ase 1 (*EhRdRP1*) gene was unusual in that the trigger fusion did not result in generation of small RNAs; commensurate with lack of small RNAs, no subsequent gene silencing was noted (36).

To understand the mechanisms of trigger-induced gene silencing, we aimed to investigate whether there is a correlation between small RNA generation and heterochromatin marks. In *Entamoeba*, plasmid DNA is maintained episomally and does not integrate; thus, we can assess the gene expression and histone modifications at the episomal plasmid (which contains the trigger-gene fusion) and also at the endogenous chromosomal location. We chose to study the 19T-ROM1 cell line (in which small RNAs are generated and *ROM1* has stable long term silencing) and compared it to a parasite strain in which *ROM1* is overexpressed with a Myc fusion (Myc-ROM1). These cell lines were chosen for comparison because both cell lines were (i) under the same drug selection pressure, (ii) contained an episomal plasmid, and (iii) had episomal plasmid expression driven by the same promoter (Fig. 3*A*). First, we performed RT-PCR experiments to compare the expression level of *ROM1* in 19T-ROM1 and Myc-ROM1 cell lines. We used primer pairs that can assess the total level of *ROM1* transcripts (*i.e.* ROM1 transcribed from both the chromosomal gene and the episomal plasmid). We observed substantial reduction in *ROM1* expression in 19T-ROM1 cells *versus* high levels in the Myc-ROM1 cell line (Fig. 3*B*). Next, we evaluated the level of *ROM1* transcript generated only from the plasmid in each of the two lines (labeled episomal *ROM1* to distinguish from *ROM1* transcript expressed from genomic locus). We identified a very low expression level of episomal *ROM1* in the 19T-ROM1 cell line as compared with the high expression level in the Myc-ROM1 cell line (Fig. 3*B*).

To evaluate the level of H3K27, H3K27Me2, and Ago2-2 protein depositions at *ROM1* loci in the two cell lines, we performed chromatin immunoprecipitation experiments followed by PCR analysis. First, we monitored the enrichment levels at the episomal *ROM1* silencing construct. We found statistically significant enrichment of H3K27 (80.6% $\pm$ 5.2; $p = 0.00001$) and H3K27Me2 (54.9% $\pm$ 5.5; $p = 0.0002$) at the episomal locus containing the silenced episomal *ROM1* in 19T-ROM1 cells relative to low abundance at the expressed *RPL21* genomic locus (18.1 $\pm$ 4.1% and 9.8 $\pm$ 4.3%, respectively) (Fig. 4*A*). In contrast, the Myc-ROM1 cell line showed no significant histone enrichment at the episomal overexpression plasmid compared with *RPL21* ($p = 0.2$ for H3K27; $p = 0.1$ for H3K27Me2) (Fig. 4*B*). H3K27 and H3K27Me2 histone enrichment at the silencing construct in 19T-ROM1 were 4-fold increased compared with the highly expressed plasmid in Myc-ROM1 cells (Fig. 4*C*). However, we could not detect significant enrichment of Ago2-2 at the episomal construct in 19T-ROM1 ($p = 0.1$). Deposition of H3K27Me3 on an episome has been reported recently in Kaposi sarcoma-associated *Herpesvirus* and linked to gene silencing (48).

Next we asked whether the profile of H3K27, H3K27Me2, and Ago2-2 deposition at the chromosomal *ROM1* locus differs from that determined at the episomal plasmid. We amplified a chromosomal DNA fragment of *ROM1* (including a promoter region and 5′ coding portion). We determined that in the 19T-ROM1 (*ROM1* silenced), this chromosomal *ROM1* region was significantly enriched for H3K27 (58.7 $\pm$ 3.9%; $p = 0.0001$), H3K27Me2 (28.5% $\pm$ 3.3; $p = 0.02$), and Ago2-2 (47.5 $\pm$ 6.5%; $p = 0.01$) compared with the same locus in Myc-ROM1 cells, in which *ROM1* is overexpressed (Fig. 4, *D* and *E*). Interestingly, the H3K27Me2 abundance was very high at this chromosomal *ROM1* locus (10-fold enriched compared with the same locus in Myc-ROM1 cells) indicating that the silenced *ROM1* locus was highly enriched with the repressive H3K27Me2 mark (Fig. 4*F*). Similar results were noted with the analyses of a 5′-coding portion of *ROM1* (Fig. 4, *G–I*). The observed Ago2-2 enrichment at the chromosomal locus was in contrast to the results noted on the silenced episomal plasmid. Lack of substantial Ago2-2 enrichment at the coding region while detecting moderate enrichment at the chromosomal fragment, which includes a promoter region, may imply a transient role for Ago2-2 in an early stage of RNAi-mediated gene silencing. The results indicate that trigger-induced small RNA gene silencing in *E. histolytica* is associated with substantial deposition of repressive H3K27Me2 at silenced loci and a moderate amount of Ago2-2 at the chromosomally silenced locus when the genomic loci are

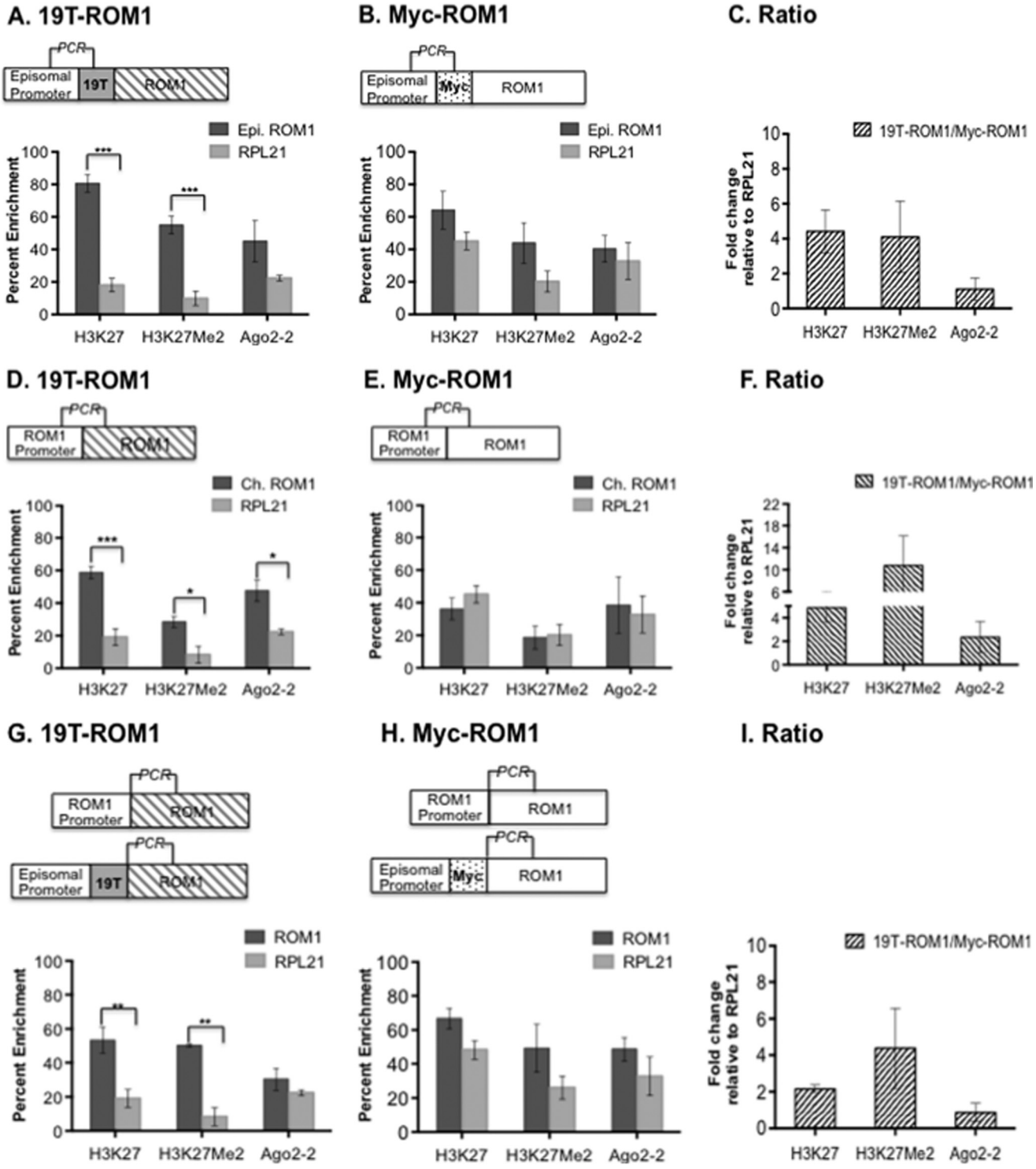

FIGURE 4. **Both episomal and chromosomal silenced *ROM1* genes are enriched in repressive marks.** 19T-ROM1 and Myc-ROM1 cells were cross-linked with formaldehyde and the extracted nuclear lysate was immunoprecipitated with control IgG or antibodies specific for *E. histolytica* H3K27, H3K27Me2, or *EhAgo2-2*. Protein enrichment, with subtracted IgG background, is displayed as a percentage of the enriched region relative to input DNA. Likewise, enrichment levels measured at constitutively expressed *RPL21*. *A,* a significant increase of the 19T-ROM1 episomal region enriched with H3K27 and repressive H3K27Me2 as compared with RPL21. *B,* corresponding Myc-ROM1 episomal region with levels of protein deposits similar to *RPL21*. *C,* 4-fold increase of 19T-ROM1 episomal regions enriched with H3K27 and repressive H3K27Me2 as compared with Myc-ROM1. The chart displays the ratio of *RPL21*-normalized enrichment values at episomal region shown in *A* relative to normalized levels in *B* (*i.e.* normalized *A*/*B*). *D,* 19T-ROM1, significant increase in chromosomal ROM1 region enriched with H3K27, H3K27Me2, or Ago2-2. *E,* Myc-ROM1, chromosomal *ROM1* enriched with similar protein levels as RPL21. *F,* significant increase in the amount of chromosomal *ROM1* regions enriched with H3K27 (5-fold) and repressive H3K27Me2 (10-fold) as compared with the same region in Myc-ROM1 cells. The chart displays the ratio of the *RPL21*-normalized enrichment values at the chromosomal *ROM1* region shown in *D* relative to normalized levels in *E* (*i.e.* normalized *D*/*E*). Data represent mean ± S.E. of at least three independent ChIP experiments. *, $p < 0.05$; **, $p < 0.01$; ***, $p < 0.001$.

under active process of trigger-silencing (*i.e.* silencing construct is under continued selection).

Long Term Gene Silencing of ROM1 Correlates with Elevated Levels of H3K27Me2 Deposition—It has been confirmed that distinct chromatin-remodeling complexes are responsible for maintaining long term gene repression at particular loci (49). *E. histolytica* trophozoites are able to maintain gene silencing for years after removal of the silencing construct as shown in both the G3 strain (37) and the trigger-ROM1 cell lines (35). We attribute this feature to possible inheritable epigenetics. To study the proposed inheritable epigenetics of prolonged gene silencing, we analyzed 19T-ROM1$^{\text{No plasmid}}$ compared with a control cell line where *ROM1* is expressed at normal levels. RT-PCR analysis confirmed that the cells had stable down-regulation of *ROM1* despite loss of the silencing construct, with *ROM1* silencing at comparable levels to that when plasmid was present (Fig. 5, *A* and *B*). 19T-ROM1$^{\text{No plasmid}}$ cells maintained production of sRNA although at levels moderately lower than the cells with trigger plasmid (35). Using ChIP we determined protein depositions at the silenced *ROM1* chromosomal gene locus by investigating a DNA fragment of *ROM1* that included a promoter region and 5′ coding portion. *ROM1* locus showed a significant enrichment of both H3K27 (61.6 ± 9%, $p = 0.01$) and H3K27Me2 (48.6 ± 11%; $p = 0.02$) relative to *RPL21* (28.7 ± 7.6% and 16.4 ± 5%, respectively) (Fig. 5, *C–E*), the increased levels were 2-fold (for H3K27) and almost 3-fold (for H3K27Me2) compared with wild type cells. Interestingly, the same chromosomal region showed higher levels of histone enrichment in the presence of a silencing construct (Fig. 4*F*). Trigger-mediated silencing is transcription dependent with no silencing in a promoter-less Trigger-*ROM1* construct (35). The chromosomal locus of *ROM1* seems to be loaded with H3K27Me2 in a manner that permits continuous small RNA production. In contrast to the 19T-ROM1 cell line, we did not detect a significant Ago2-2 enrichment at the chromosomal *ROM1* locus in 19T-ROM1$^{\text{No plasmid}}$ cells (57 ± 14.8%; $p = 0.1$). Furthermore, we looked at a coding region of *ROM1* and found that the levels of H3K27Me2 were enriched to 20-fold relative to wild type cells and H3K27 deposition was 4-fold higher, whereas Ago2-2 did not show a significant increase (Fig. 5, *F–H*). The substantial higher enrichment of H3K27Me2 at *ROM1* coding regions in the absence of a trigger-plasmid suggests that adaptation takes place after the silencing construct is removed. The data imply that Ago2-2 deposition may be needed for the initiation phase of silencing, but is not required for maintaining the silencing, whereas larger depositions of H3K27Me2 are needed in the absence of a trigger to maintain prolonged gene repression.

Trigger Silencing of Ago2-2 Is Incomplete: Silencing and H3K27Me2 Enrichment at the Episomal Plasmid but a Transcriptionally Active Chromosomal Locus with No H3K27Me2 Enrichment—The *E. histolytica* genome encodes several genes thought to be involved in the RNAi gene silencing pathway including three Argonaute proteins, Ago2-1, Ago2-2, and Ago2-3 as well as two RdRP genes and a single *RNase III* gene (50). All RNAi pathway genes we tested (*Ago2-1*, *Ago2-2*, *Ago2-3*, and *RNase III*) were resistant to trigger-mediated gene silencing despite generation of abundant and functional small RNAs (36). For our analysis, we focused on the *Ago2-2* locus to determine whether there was differential silencing of the episome and chromosomal copy of *Ago2-2* and whether H3K27, H3K27Me2, or Ago2-2 deposits occurred at either the episome or chromosomal locations. To determine the levels of *Ago2-2* transcript, we performed RT-PCR experiments in cells with the 19T-Ago2–2 silencing construct and compared the results to Ago2-2 expression levels in cells that contain Myc-Ago2-2 expressing plasmid (Fig. 6*A*). Interestingly, we found reduced levels of the episomal 19T-Ago2-2 transcript, which means the episomal *Ago2-2* has lower expression compared with another episomal plasmid driven by the same promoter (Myc-Ago2-2) (Fig. 6*B*). When we tested the overall expression of *Ago2-2* using primers that anneal to the coding region of *Ago2-2* (thus amplifying signal from both episomal and genomic generated transcripts), we did not see a difference in gene expression in 19T-Ago2-2 cells compared with wild type cells. Our results indicate that in the 19T-Ago2-2 cells, whereas expression of the episomal copy is somewhat repressed, the genomic *Ago2-2* locus is transcriptionally active. The episomal silencing of *Ago2-2* and the abundant functional small RNAs to *Ago2-2* raises the question about whether H3K27, H3K27Me2, and Ago2-2 proteins deposit on episomal Ago2-2 locus to induce episomal silencing. To answer this question, we performed ChIP experiments on 19T-Ago2-2 and Myc-Ago2-2 cell lines. ChIP-PCR analysis of the episomal 19T-Ago2-2 locus showed significant enrichment of H3K27 (77.3 ± 5.3%; $p = 0.002$) and H3K27Me2 (67.1 ± 6.5%; $p = 0.007$) as compared with *RPL21* (24.6 ± 8.9% and 20.1 ± 9.9%, respectively), whereas Myc-Ago2-2 was not significantly enriched with histones (Fig. 7, *A* and *B*). Enrichment levels of H3K27Me2 at 19T-Ago2-2 were 6 times greater than that at Myc-Ago2-2 (Fig. 7*C*). Similar to the 19T-ROM1 cell line, we did not observe an episomal enrichment of *Ago2-2*. These results indicate that the 19-Trigger fusion to *Ago2-2* was able to induce repressive H3K27Me2 deposits at the episomal locus of Ago2-2 to repress transcription. However, the chromosomal locus did not show any significant enrichment of H3K27, H3K27Me2, or Ago2-2, which matches the high transcriptional activity at that locus and is consistent with similar results of the *Ago2-2* coding region (Fig. 7, *D–I*). Why the chromosomal copy of *Ago2-2* does not silence despite generation of small RNAs to *Ago2-2* and silencing of the episomal copy is not clear could be due to the essential nature of *Ago2-2* or an inability of heterochromatin to assemble at the *Ago2-2* locus. Taken together the trigger-generated *Ago2-2* sRNA may induce recruitment of transcription repressive H3K27Me2 only at the episomal *Ago2-2* locus but not at the chromosomal locus, which then retains its transcription activity. Collectively, we attribute the incomplete silencing of *Ago2-2* to a small RNA-related factor or to the fact that the *Ago2-2* genetic locus is protected against TGS.

The RdRP1 Locus Is Resistant to Small RNA Generation and Silencing and Lacks H3K27Me2 Enrichment—Applying the Trigger-mediated gene silencing method to down-regulate *RdRP1* did not result in generation of small RNAs or gene silencing of *RdRP1* (36). *RdRP1* was the only gene tested to date in which the Trigger fusion did not result in small RNA generation. To further confirm the direct correlation between small

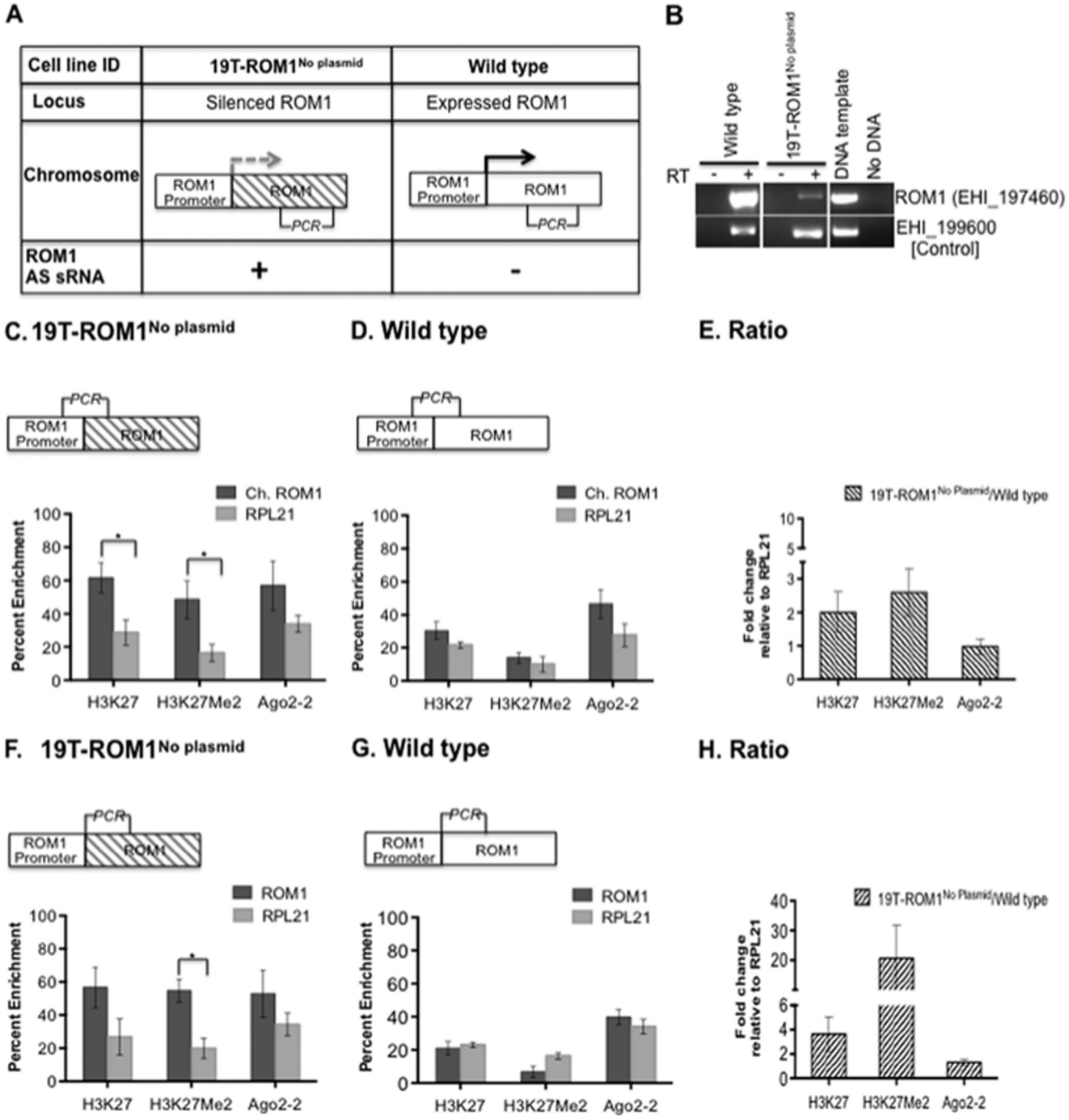

FIGURE 5. **Persistence of *ROM1* silencing after removing the trigger-silencing construct coupled with enrichment of H3K27Me2.** *A,* schematic diagram for transcriptionally inactive chromosomal *ROM1* locus in 19 trigger-*ROM1* cells that lost the silencing construct (19T-ROM1$^{\text{No plasmid}}$). Depicted is endogenously active *ROM1* locus in wild type *E. histolytica* trophozoites. *ROM1* antisense (*AS*) sRNAs are depicted in 19T-ROM1. *Striped box*, silent gene; *arrows*, transcription status; *PCR,* amplified regions in *B*. *B,* RT-PCR analysis of RNAs collected from 19T-ROM1$^{\text{No plasmid}}$ and wild type *E. histolytica* cells grown for 48 h. The analysis shows prolonged down-regulation of *ROM1* after removing the silencing construct. Transcript levels of the *EHI_199600* gene serve as a reference control. *DNA template*, genomic DNA of wild type cells. *C-H*, ChIP-PCR analysis of 19T-ROM1$^{\text{No plasmid}}$ and wild type *E. histolytica* cells shows levels of *ROM1* regions enriched with *E. histolytica* H3K27, H3K27Me2, or *EhAgo2-2*. Enriched DNA with subtracted IgG background is displayed as a percentage of input and compared with enrichment at the constitutively expressed *RPL21* gene. *C,* 19T-ROM1$^{\text{No plasmid}}$ shows a significant enrichment of H3K27 and H3K27Me2 at *ROM1*-silenced locus. *D,* wild type cells display *ROM1* expressed locus with enrichment levels similar to *RPL21*. *E,* increase in H3K27 (2-fold) or H3K27Me2 (~3-fold) enrichment in cells with maintained *ROM1* silencing as compared with wild type cells. The chart displays the ratio of RPL21-normalized enrichment values at the DNA region encoding *ROM1* shown in *C* relative to normalized levels in *D* (*i.e.* normalized *C*/*D*). *F*, 19T-ROM1$^{\text{No plasmid}}$, significant increase of ROM1 coding region enriched with repressive H3K27Me2 as compared with *RPL21*. *G*, wild type cells, levels of enriched *ROM1* coding regions are similar to *RPL21*. *H,* silenced *ROM1* coding regions enriched with repressive H3K27Me2 at 20-fold compared with wild type cells. The chart displays the ratio of the *RPL21* normalized enrichment values at the *ROM1* coding region shown in *A* relative to normalized levels in *B* (*i.e.* normalized *F*/*H*). Data represent mean ± S.E. of at least three independent ChIP experiments. *, $p < 0.05$; **, $p < 0.01$; ***, $p < 0.001$.

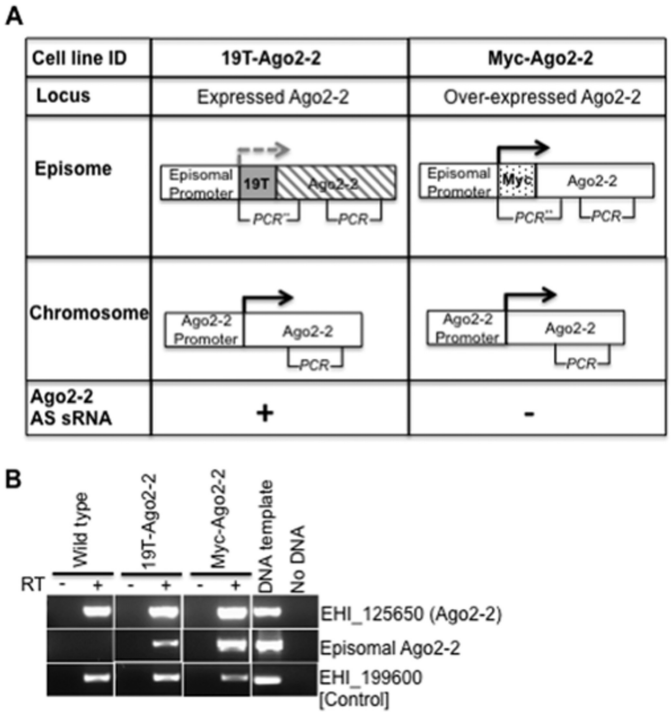

FIGURE 6. **Episomal *Ago2-2* is susceptible to trigger-mediated silencing, whereas chromosomal locus is robustly resistant.** *A,* diagram showing constructs used for silencing *Ago2-2* (*19T-Ago2-2*) or for overexpression (*Myc-Ago2-2*). Both constructs are generated from the same vector backbone and under the control of the same promoter and regulatory elements. **, episomal region; *PCR,* amplified regions of *Ago2-2* shown in *B*. *Ago2-2* antisense (*AS*) sRNAs are present in 19T-Ago2-2; *striped box*, silent gene. *B,* RT-PCR analysis of RNAs collected from 19T-Ago2-2 and Myc-Ago2-2 trophozoites. As depicted in *A*, a set of primers designed specifically to anneal to the cDNA synthesized from the construct-generated *Ago2-2* transcript to represent the levels of episomal *Ago2-2* transcript. In the same way, RT-PCR was designed to evaluate the total level of *Ago2-2* transcripts (*i.e.* transcribed from both episomal and genomic loci). Expression levels of the *EHI_199600* gene serve as a reference control. *DNA template*, genomic DNA or plasmid DNA (for episomal *Ago2-2*, only PCR product of 19T-Ago2-2 is shown). Data represent analysis of three independent biological replicates.

RNA and heterochromatin, we investigated the *RdRP1* locus in cells with an *RdRP1* silencing construct (19T-RdRP1) and cells containing a Myc-RdRP1 expressing construct (Fig. 8*A*). RT-PCR analysis confirmed that the episomal *RdRP1* locus is highly transcribed, which fits the observation that no small RNAs are generated to the *RdRP1* locus (Fig. 8*B*). We conducted chromatin immunoprecipitation experiments followed by PCR analysis to investigate protein depositions at *RdRP1* containing plasmids and chromosomal *RdRP1* locus and did not observe any specific enrichment of repressive histone modifications (Fig. 8, *C–E*). The overall lack of histone enrichment confirms that histone repressive factors correlate with small RNA abundance and gene silencing.

H3K27Me2 Deposits Interfere with RNA Polymerase II—The differential pattern of H3K27Me2 depositions led us to analyze the sites that are enriched with the repressive mark H3K27Me2, for RNA Pol II. Active transcription takes place in two substantially different phases, the formation of an active initiation complex followed by an elongation process (51). Several studies reported the interaction between the yeast heterochromatic gene silencing and transcription initiation factors as well as hindering RNA Pol II elongation by the repressive chromatin (52, 53). Here, we used *E. histolytica* strains with reduced expression of *ROM1*, whereas the silencing triggered plasmid is maintained (19T-ROM1) or removed (19T-ROM1$^{\text{No plasmid}}$). We performed immunoprecipitation experiments using specific *E. histolytica* antibody raised specifically against EhPol II subunit RBP9, which is known to be involved in transcription elongation and initiation through the interaction with other Pol II subunits (38, 54). We targeted the *ROM1* promoter and coding regions, which showed a distinguished pattern for H3K27Me2 enrichment (Figs. 4, *F* and *I*, and 5, *E* and *H*). We aimed to investigate the accessibility of those *ROM1* regions to Pol II by ChIP experiments and compare the results to Pol II enrichment at the corresponding regions of the constitutively expressed *RPL21* gene. Additionally, we used wild type cells and a Myc-ROM1 overexpressing strain as control cells where Pol II enrichment at *ROM1* and *RPL21* should be maintained at normal levels. Interestingly, we observed no significant difference of Pol II occupancy at the ROM1 promoter region in 19T-ROM1$^{\text{No plasmid}}$ cells as compared with wild type cells (1.7-fold; $p = 0.38$) (Fig. 9). In contrast, the coding region of *ROM1* showed a significant reduction of Pol II (0.26-fold $\pm$ 0.1; $p = 0.0007$). These results are the opposite of what we noted for H3K27Me2 deposition where the promoter region showed 3-fold and the coding portion displayed 20-fold enrichment (Fig. 5, *E* and *H*). This inverse Pol II/H3K27Me2 abundance implies that transcription could be initiated for the purpose of producing sRNAs, but the elongation process is inhibited when Pol II collides with the H3K27Me2 deposits at the coding region of *ROM1*. The results of 19T-ROM1 cells with the silencing construct supported our conclusion because Pol II occupancy at the *ROM1* promoter decreased significantly compared with Myc-ROM1 overexpressing strain (0.24-fold $\pm$ 0.07; $p = 0.03$). This low Pol II occupancy is consistent with the 10-fold increased deposits of H3K27Me2 at the *ROM1* promoter region (Fig. 4*F*). As expected, the coding region of *ROM1* showed a significant decrease in Pol II occupancy relative to Myc-ROM1 cells (0.32-fold $\pm$ 0.08; $p = 0.04$). The results suggest that during active trigger silencing the trigger plasmid is the primary source of transcription and sRNA production. However, in the absence of the trigger plasmid, stable silencing necessitates limited transcription of the chromosomal *ROM1* locus to ensure sRNA production and continued silencing. Collectively, amebic cells appear to adapt sRNA production, transcription inhibition, and heterochromatin formation to maintain TGS.

Discussion

We describe the first molecular mechanism that couples transcriptional gene silencing and the RNAi pathway in the protozoan parasite *E. histolytica*. We identify H3K27Me2 as an amebic repressive epigenetic mark associated with silenced loci. We identify two distinct phases of RNAi-mediated transcriptional gene silencing (Fig. 10). In the initial phase, where the silencing Trigger is present, concurrent depositions of H3K27Me2 and Argonaute protein appear to repress gene transcription. In the second and prolonged gene silencing phase where the RNAi-Trigger is absent, efficient silencing is maintained apparently independent of Argonaute protein deposition, but by increased deposits of repressive H3K27Me2 on

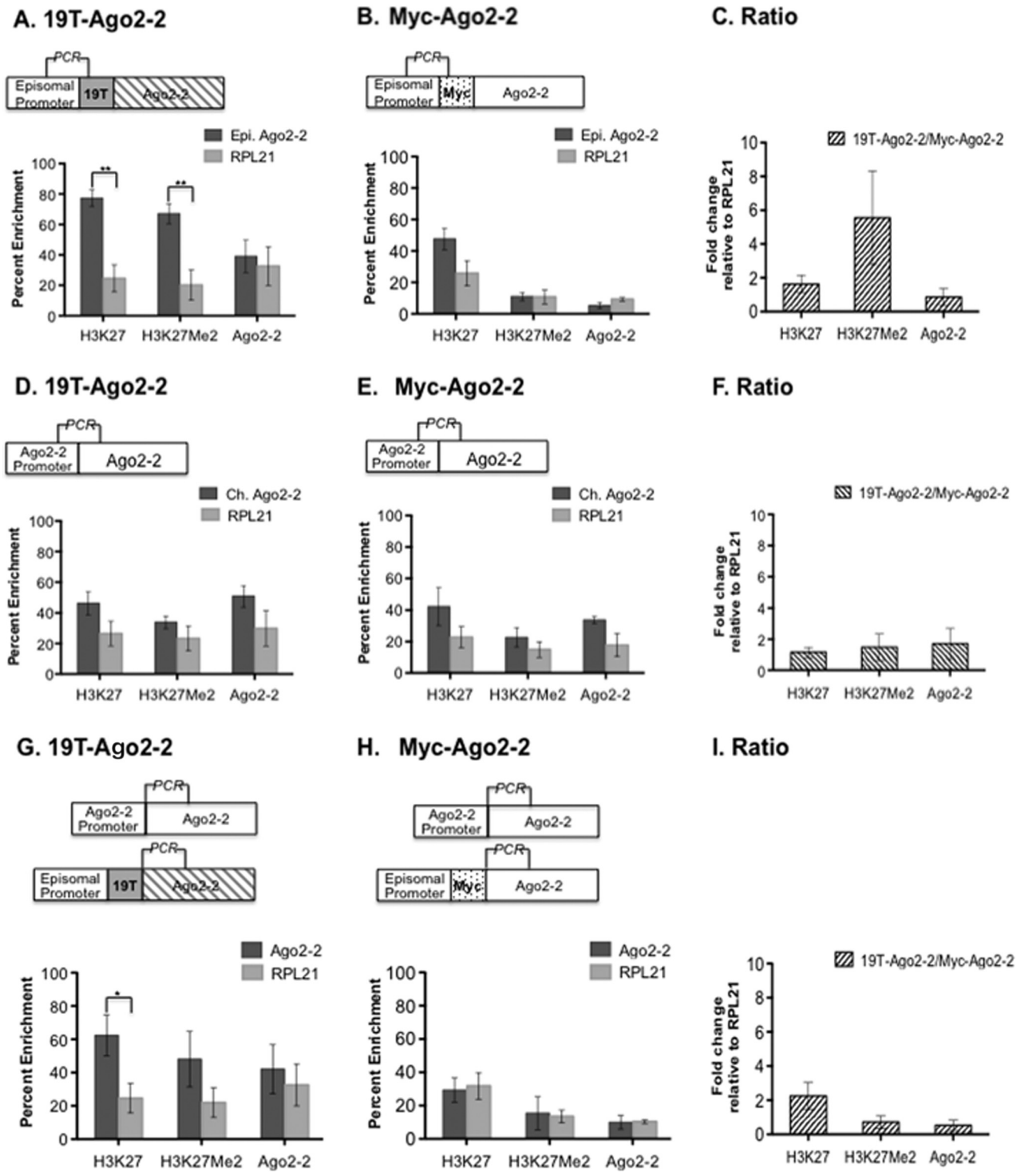

FIGURE 7. **Repressive H3K27Me2 enriches only episomal *Ago2-2*.** ChIP-PCR analysis of 19T-Ago2-2 and Myc-Ago2-2 cells demonstrate deposits of *E. histolytica* proteins H3K27, H3K27Me2, or EhAgo2-2. Enriched DNA is displayed as percentages of input DNA after subtracting IgG background and compared with enrichment at the constitutively expressed *RPL21* gene. *A,* significant enrichment of H3K27 and H3K27Me2 at the silenced episomal locus of *Ago2-2*. *B,* overexpressed episomal *Ago2-2* gene is enriched with protein levels similar to *RPL21*. *C,* episomal silenced *Ago2-2* enriched with repressive H3K27Me2 at 6-fold more than Myc-Ago2-2. The chart displays the ratio of the *RPL21*-normalized enrichment values at the DNA region encoding ROM1 shown in *A* relative to normalized levels in B (*i.e.* normalized *A*/*B*). *D* and *E,* results of ChIP-PCR analysis shows the absence of any significant protein deposits at the chromosomal *Ago2-2* locus that is not silenced in 19T-Ago2-2 (*D*) or expressed in Myc-Ago2-2 cells (*E*). *F,* ratio of RPL21 normalized levels of *D* to *E* indicates similar protein enrichment at chromosomal *Ago2-2* locus in both 19T-Ago2-2 and Myc-Ago2-2 cells. *G,* in 19T-Ago2-2 parasites, the coding region of *Ago2-2* lacks repressive H3K27Me2 or Ago2-2 enrichment. *H,* in Myc-Ago2-2, the coding region of Ago2-2 was enriched with protein quantities similar to *RPL21*. *I,* the chart displays the ratio of the *RPL21* normalized enrichment at the *Ago2-2* coding region shown in *G*, relative to normalized levels in *H* (*i.e.* normalized *G*/*H*). Data represent mean ± S.E. of three independent ChIP experiments. *, $p < 0.05$; **, $p < 0.01$; ***, $p < 0.001$.

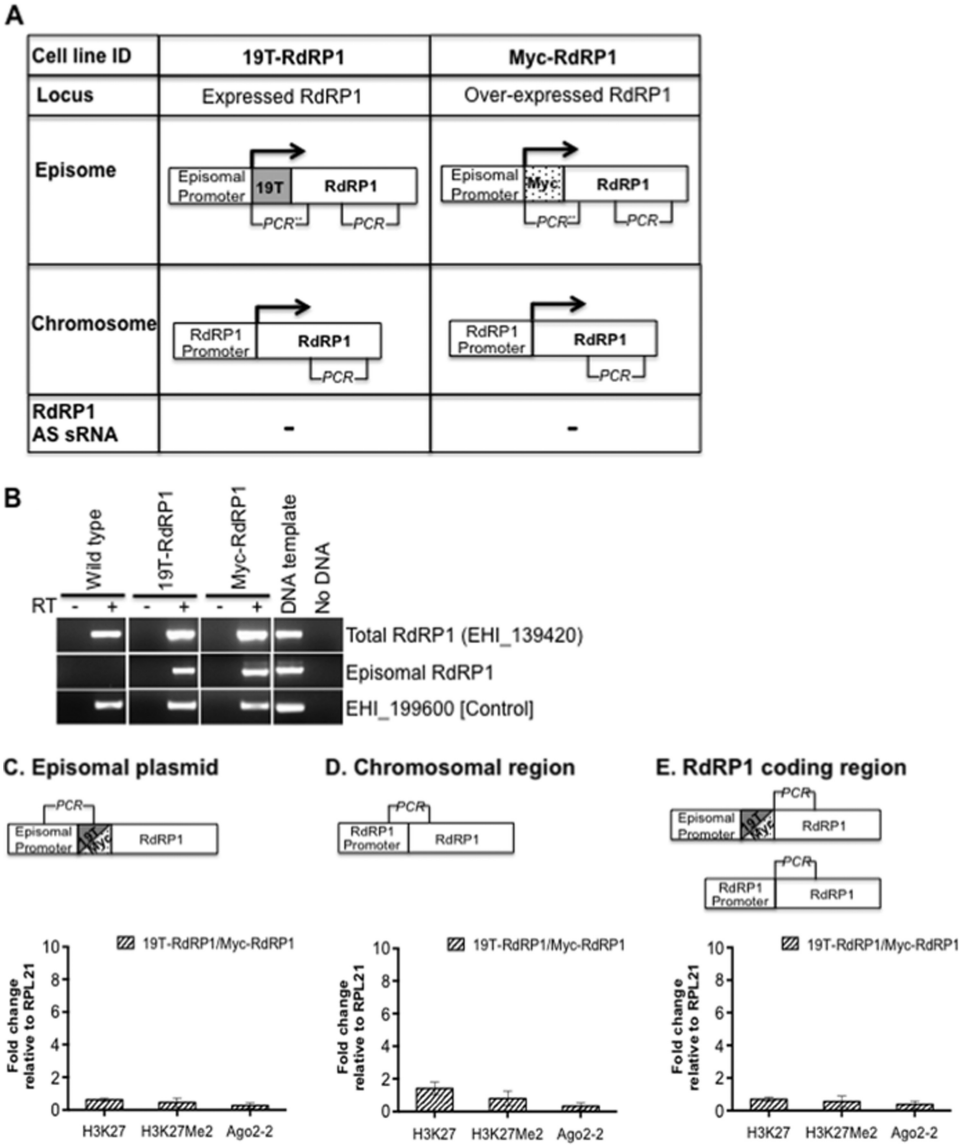

FIGURE 8. **Both the episomal and chromosomal RdRP1 loci are resistant to trigger silencing and are not enriched with repressive epigenetic marks.** *A,* schematic diagram of constructs designed to silence *RdRP1* (*19T-RdRP1*) or overexpress it (*Myc-RdRP1*). Both constructs are built from the same vector backbone and are under control of the same promoter and regulatory elements; **, episomal region; *PCR,* amplified regions of *RdRP1* shown in *B*. 19T-RdRP1 cells do not have antisense sRNAs. *B,* RT-PCR analysis of RNAs collected from 19T-RdRP1 and Myc-RdRP1 *E. histolytica* trophozoites grown for 48 h. Up-regulation of the *RdRP1* transcript shown with both primer sets designed specifically to anneal to cDNA synthesized from the construct-generated *RdRP1* transcript (*i.e.* episomal *RdRP1*) or cDNA strands were made from episomal and chromosomal *RdRP1* transcripts (total *RdRP1*). *DNA template,* genomic DNA or plasmid DNA (for episomal *RdRP1*; only PCR product of Myc-RdRP1 is shown). Expression levels of the *EHI_199600* gene serve as a reference control. Data represent analysis of three independent biological replicates. *C-E*, ChIP-PCR analyses of 19T-RdRP1 and Myc-RdRP1 cells represent deposition levels of H3K27, H3K27Me2, or EhAgo2–2. Shown is the ratio of *RPL21* normalized levels of the indicated enriched DNA of 19T-RdRP1 cells were calculated relative to that of Myc-RdRP1. Diagrams depict different amplified regions; *19T/Myc*, plasmids of 19T-RdRP1 or Myc-RdRP1. Results of ChIP-PCR analysis showing the absence of any protein enrichment. Data represent three independent ChIP experiments. *, $p < 0.05$; **, $p < 0.01$; ***, $p < 0.001$.

coding regions. Thus, methylated histones appear to be the major mediator for prolonged transcriptional silencing. Moreover, we identified an inverse correlation between Pol II and H3K27Me2 enrichment at silenced loci indicating an associated impairment in transcription initiation and elongation. The Pol II enrichment at the promoter regions was determined only in the absence of the trigger-silencing plasmid indicating that low level transcription is maintained to ensure ongoing sRNA production. The repressive H3K27Me2 epigenetic mark characterizes the molecular interplay between the amebic RNAi pathway and heterochromatin-mediated transcriptional gene silencing in a deep-branching eukaryote.

In *E. histolytica* G3 strain it was previously noted that RNAi-silenced loci had increased histone H3 occupancy (33, 37). However, these studies could not address identification of specific repressive histone marks as the reagents for the study were not available. It has been reported in other biological systems that enrichment of methylated H3K27 associates with gene repression (14, 43). Using newly generated reagents, we have identified that *E. histolytica* also contains this repressive epigenetic mark, which deposits at RNAi-silenced loci. Identification of a repressive H3K27Me2 suggests the presence of a functional epigenetic machinery in *E. histolytica*, which reinforces the identification of potential histone methyltransferases, histone

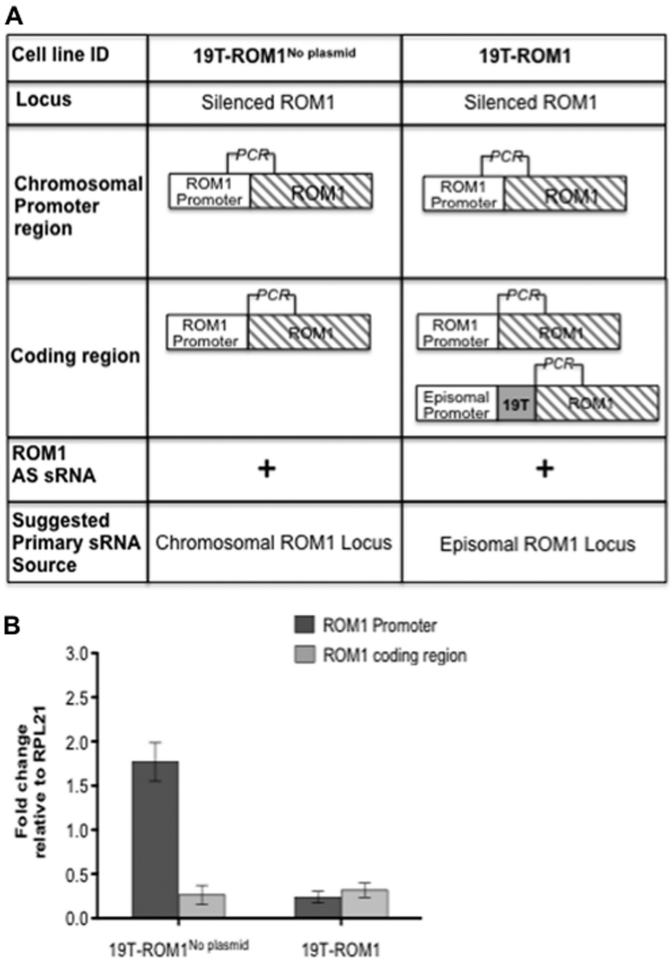

FIGURE 9. **RNA Pol II enrichment is inversely correlated with H3K27Me2 deposition.** *A,* schematic diagram for ROM1 locus in 19T-ROM1$^{\text{No plasmid}}$ and 19T-ROM1 cells. *PCR,* regions amplified in ChIP-PCR in *B* to scan for Pol II. *ROM1* antisense (*AS*) sRNAs and their postulated transcription origin are depicted. *Striped box*, silent gene. *B,* ChIP-PCR analysis of 19T-ROM1$^{\text{No plasmid}}$ (control strain: wild type cells) and 19T-ROM1 (control strain: Myc-ROM1 cells). Shown are levels of the *ROM1* promoter and coding regions enriched with *E. histolytica* Pol II. Fold-change of Pol II enrichment relative to the control strain was calculated as a percentage of input after subtracting IgG background; the values were normalized to Pol II-enriched *RPL21* promoter or coding region. 19T-ROM1$^{\text{No plasmid}}$ shows similar levels of Pol II at the *ROM1* promoter region relative to wild type cells (1.7-fold; $p = 0.2$) and significant reduction at the ROM1 coding portion. 19T-ROM1 cells with plasmid display a significant decrease in Pol II at both *ROM1* promoter and coding regions. Data represent mean and S.E. of three independent ChIP experiments. *, $p < 0.05$; **, $p < 0.01$; ***, $p < 0.001$.

modifying enzymes, DNA methylation components, and chromodomain containing proteins in the *Entamoeba* genome (55). Future efforts to characterize the RNA-induced transcriptional silencing complex will identify the molecular mediators of interactions between the Argonaute protein and histone modifying enzymes.

The ability of *E. histolytica* trophozoites to maintain silencing after trigger removal is a good opportunity to dissect the determinants for prolonged silencing. Our data indicate that the chromosomal *ROM1* locus has different patterns of histone methylation in the presence or absence of the trigger-silencing construct. In 19T-ROM1 cells, where the silencing construct is present, we detected enrichment of 10-fold of H3K27Me2 at chromosomal regions containing a portion of the *ROM1* endogenous promoter. However, after plasmid removal despite active silencing, the same chromosomal region had only 3-fold H3K27Me2 enrichment. Very interestingly, the opposite scenario was observed at *ROM1* coding regions. The H3K27Me2 abundance at coding regions was increased 4-fold when the plasmid was present, compared with a 10-fold increase after plasmid removal. This observation indicates an inverse correlation between transcriptional activity and H3K27Me2 deposits, which is in agreement with the observation that trigger silencing is transcription dependent (35). In the absence of the silencing construct, there is a need for transcription of the gene locus as a source to produce small RNAs; thus, some accessibility of the promoter may be required to facilitate small RNA production. Our conclusion is supported by the results of Pol II ChIP experiments in which reduced levels of Pol II are in agreement with increased H3K27Me2 deposition. However, Pol II seems to access the promoter region easily in the absence of trigger plasmid, which may be due to a requirement for limited transcription to continuously generate sRNAs. In *S. pombe*, plants, and human, RNAi interplays with repressive H3K9Me-mediated heterochromatin assembly in a transcription-dependent manner (56–58). This differential pattern of H3K27Me2 enrichment demonstrates that amebic cells similarly modulate RNAi-mediated gene silencing. Heterochromatin spreading into neighboring regions has been described in several cases including yeast and plant (59–61, 72). Likely, the *E. histolytica* deposition of the H3K27Me2 mark in the promoter region and in the gene body might be an indication for heterochromatin spreading status.

The interplay between Argonaute proteins and heterochromatin-induced factors has been studied in multiple systems. In *D. melanogaster*, Argonaute proteins are implicated in heterochromatin-mediated silencing via a role in targeting and recruitment of histone modifying enzymes and chromodomain proteins (28, 62), and in *S. pombe* Ago1 deposits at genomic loci where other RNAi components enrich to contribute to heterochromatin silencing (63). Additionally, disruption of RNAi affects both establishment and maintenance of heterochromatin at centromeres (64). Human Argonaute proteins, AGO1 and AGO2, mediate TGS via interactions with lysine methyltransferases specific for methylation of H3K9 and H3K27 (65, 66). Our investigation of trigger-induced silenced genes demonstrated enrichment of Ago2-2 only at the silenced chromosomal *ROM1* locus in the presence of the silencing construct. Despite silencing, the episomal plasmids lack Ago2-2 enrichment suggesting that targeting Ago2-2 is transient or highly specific.

Why the *Ago2-2* silencing construct could not silence the chromosomal *Ago2-2* locus despite generation of functional small RNAs is not known. One simple possibility is that Ago2-2 has an essential role and thus its genomic locus is protected from epigenetic modifications. Inhibition of euchromatin conversion to heterochromatin has been described in *S. pombe* and *Arabidopsis thaliana*, where it is mediated via Jumonji C domain-containing proteins (67, 68). Another possibility is that *Ago2-2* small RNAs do not reach the *Ago2-2* chromosomal locus due to a nonfunctional Ago2-2·sRNA complex. For example, the complex may fail to properly position thus failing to

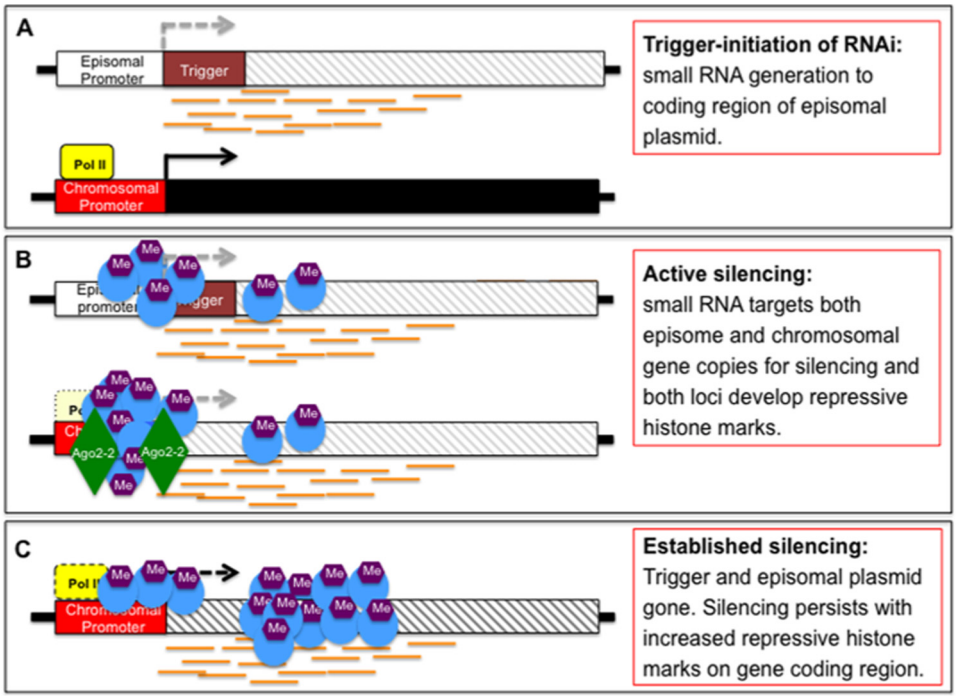

FIGURE 10. **Proposed model for the mechanism linking RNAi gene silencing and repressive histone-mediated transcriptional gene silencing.** *A*, description of the trigger approach. A region (trigger) of an endogenously silenced gene with abundant antisense sRNA fused to a full-length gene (*e.g. ROM1*). At the episome, the trigger induces generation of a small RNAs map specifically to the fused gene. Active transcription of the chromosomal *ROM1* locus is depicted by Pol II and a *solid black arrow*. *B,* active phase of transcriptional gene silencing in which small RNAs induce deposition of repressive H3K27Me2 at the episomal trigger-silenced gene. The chromosomal copy of the target gene is subsequently repressed with associated enrichment of repressive H3K27Me2 and Ago2-2. Repressed transcription of chromosomal *ROM1* locus depicted by the *dashed gray arrow*. *C,* established TGS silencing occurs when triggered silencing persists despite trigger plasmid removal. Long term gene silencing is maintained by large deposits of repressive H3K27Me2 on the gene-coding region, but is not associated with substantial Ago2-2 deposition. Limited transcription of the chromosomal locus is retained, shown by a *dashed black arrow*, with decreased amounts of repressive H3K27Me2 at the promoter region and a commensurate increase in the abundance of Pol II. Small RNAs (*tan lines*), RNA polymerase II (*yellow box*), Ago2-2 (*green diamond*), and H3K27Me2 (*blue dot with Me*).

facilitate recruitment of repressive chromatin factors. In cultured mammalian cells, a single-base difference in the positioning of a synthetic small RNA can activate or inhibit transcription (69). Alternatively, the *Ago2-2* small RNAs may not load well into the silencing complex. Interestingly, Northern blot analysis in the 19T-Ago2-2 cells showed that the majority of *Ago2-2* small RNAs appear to be of a larger size compared with small RNAs generated to *ROM1* (36). The functional meaning of this small RNA size discrepancy needs further investigation. Given that each Argonaute protein has very specific requirements for small RNA association, it is possible that the larger small RNAs generated against *Ago2-2* do not load productively into Ago2-2 and thus cannot mediate gene silencing (70). In *Drosophila,* it has been demonstrated that modifications of the 3′ terminus of siRNAs and miRNAs are coupled to efficient assembly into Ago2-RNA-induced silencing complex (71). Future studies to understand the role of Ago2-2 (and RdRP1) in the RNAi pathway as well the requirements for their activity may explain the higher degree of resistance of these genes to gene silencing.

Our efforts are the first to shed light on the molecular mechanism of RNAi-regulated TGS in *E. histolytica*. We introduce strong evidence for H3K27Me2 as a repressive histone mark in *E. histolytica* and point to a crucial role for heterochromatin assembly in RNAi-mediated TGS in ameba. Identification of factors that mediate the RNA-induced transcriptional silencing complex is of a high priority for future efforts.

Author Contributions—B. F. and U. S. conceived and coordinated the study and wrote the paper. B. F. designed, performed, and analyzed the experiments in the paper. All authors reviewed the results and approved the final version of the manuscript.

Acknowledgments—We gratefully thank all members of the Singh lab for their helpful input. We are particularly indebted to Drs. Ehrenkaufer and Zhang for critical reading of the paper. We also thank Dr. Wu for allowing use of a sonicator. We acknowledge Dr. Sudha Bhattacharya for sharing EhRNA polymerase II antibody (anti-RPB9 antibody).

References

1. Bernstein, B. E., Mikkelsen, T. S., Xie, X., Kamal, M., Huebert, D. J., Cuff, J., Fry, B., Meissner, A., Wernig, M., Plath, K., Jaenisch, R., Wagschal, A., Feil, R., Schreiber, S. L., and Lander, E. S. (2006) A bivalent chromatin structure marks key developmental genes in embryonic stem cells. *Cell* **125,** 315–326
2. Sharma, S., Kelly, T. K., and Jones, P. A. (2010) Epigenetics in cancer. *Carcinogenesis* **31,** 27–36
3. Shi, Y. (2007) Histone lysine demethylases: emerging roles in development, physiology and disease. *Nat. Rev. Genet.* **8,** 829–833
4. Bazer, F. W., Wu, G., Spencer, T. E., Johnson, G. A., Burghardt, R. C., and Bayless, K. (2010) Novel pathways for implantation and establishment and maintenance of pregnancy in mammals. *Mol. Hum. Reprod.* **16,** 135–152
5. Heard, E., and Disteche, C. M. (2006) Dosage compensation in mammals: fine-tuning the expression of the X chromosome. *Genes Dev.* **20,** 1848–1867
6. Djupedal, I., and Ekwall, K. (2009) Epigenetics: heterochromatin meets

RNAi. *Cell Res.* **19,** 282–295
7. Chan, F. L., and Wong, L. H. (2012) Transcription in the maintenance of centromere chromatin identity. *Nucleic Acids Res.* **40,** 11178–11188
8. Boros, J., Arnoult, N., Stroobant, V., Collet, J. F., and Decottignies, A. (2014) Polycomb repressive complex 2 and H3K27me3 cooperate with H3K9 methylation to maintain heterochromatin protein 1α at chromatin. *Mol. Cell. Biol.* **34,** 3662–3674
9. Volpe, T. A., Kidner, C., Hall, I. M., Teng, G., Grewal, S. I., and Martienssen, R. A. (2002) Regulation of heterochromatic silencing and histone H3 lysine-9 methylation by RNAi. *Science* **297,** 1833–1837
10. Bannister, A. J., and Kouzarides, T. (2011) Regulation of chromatin by histone modifications. *Cell Res.* **21,** 381–395
11. Chujo, T., and Scott, B. (2014) Histone H3K9 and H3K27 methylation regulates fungal alkaloid biosynthesis in a fungal endophyte-plant symbiosis. *Mol. Microbiol.* **92,** 413–434
12. Jørgensen, S., Schotta, G., and Sørensen, C. S. (2013) Histone H4 lysine 20 methylation: key player in epigenetic regulation of genomic integrity. *Nucleic Acids Res.* **41,** 2797–2806
13. Kotake, Y., Cao, R., Viatour, P., Sage, J., Zhang, Y., and Xiong, Y. (2007) pRB family proteins are required for H3K27 trimethylation and Polycomb repression complexes binding to and silencing p16INK4α tumor suppressor gene. *Genes Dev.* **21,** 49–54
14. Plath, K., Fang, J., Mlynarczyk-Evans, S. K., Cao, R., Worringer, K. A., Wang, H., de la Cruz, C. C., Otte, A. P., Panning, B., and Zhang, Y. (2003) Role of histone H3 lysine 27 methylation in X inactivation. *Science* **300,** 131–135
15. Furuhashi, H., Takasaki, T., Rechtsteiner, A., Li, T., Kimura, H., Checchi, P. M., Strome, S., and Kelly, W. G. (2010) Trans-generational epigenetic regulation of *C. elegans* primordial germ cells. *Epigenetics Chromatin* **3,** 15
16. Rechtsteiner, A., Ercan, S., Takasaki, T., Phippen, T. M., Egelhofer, T. A., Wang, W., Kimura, H., Lieb, J. D., and Strome, S. (2010) The histone H3K36 methyltransferase MES-4 acts epigenetically to transmit the memory of germline gene expression to progeny. *PLoS Genet.* **6,** e1001091
17. Lyko, F., Beisel, C., Marhold, J., and Paro, R. (2006) Epigenetic regulation in *Drosophila*. *Curr. Top. Microbiol. Immunol.* **310,** 23–44
18. Matzke, M. A., and Birchler, J. A. (2005) RNAi-mediated pathways in the nucleus. *Nat. Rev. Genet.* **6,** 24–35
19. Batista, T. M., and Marques, J. T. (2011) RNAi pathways in parasitic protists and worms. *J. Proteomics* **74,** 1504–1514
20. Fire, A., Xu, S., Montgomery, M. K., Kostas, S. A., Driver, S. E., and Mello, C. C. (1998) Potent and specific genetic interference by double-stranded RNA in *Caenorhabditis elegans*. *Nature* **391,** 806–811
21. Ghildiyal, M., and Zamore, P. D. (2009) Small silencing RNAs: an expanding universe. *Nat. Rev. Genet.* **10,** 94–108
22. Vance, V., and Vaucheret, H. (2001) RNA silencing in plants: defense and counterdefense. *Science* **292,** 2277–2280
23. Liu, X., Jiang, F., Kalidas, S., Smith, D., and Liu, Q. (2006) Dicer-2 and R2D2 coordinately bind siRNA to promote assembly of the siRISC complexes. *RNA* **12,** 1514–1520
24. Castel, S. E., and Martienssen, R. A. (2013) RNA interference in the nucleus: roles for small RNAs in transcription, epigenetics and beyond. *Nat. Rev. Genet.* **14,** 100–112
25. Tomari, Y., Du, T., and Zamore, P. D. (2007) Sorting of *Drosophila* small silencing RNAs. *Cell* **130,** 299–308
26. Maison, C., Bailly, D., Peters, A. H., Quivy, J. P., Roche, D., Taddei, A., Lachner, M., Jenuwein, T., and Almouzni, G. (2002) Higher-order structure in pericentric heterochromatin involves a distinct pattern of histone modification and an RNA component. *Nat. Genet.* **30,** 329–334
27. Mochizuki, K., Fine, N. A., Fujisawa, T., and Gorovsky, M. A. (2002) Analysis of a piwi-related gene implicates small RNAs in genome rearrangement in tetrahymena. *Cell* **110,** 689–699
28. Pal-Bhadra, M., Leibovitch, B. A., Gandhi, S. G., Chikka, M. R., Rao, M., Bhadra, U., Birchler, J. A., and Elgin, S. C. (2004) Heterochromatic silencing and HP1 localization in Drosophila are dependent on the RNAi machinery. *Science* **303,** 669–672
29. Reinhart, B. J., and Bartel, D. P. (2002) Small RNAs correspond to centromere heterochromatic repeats. *Science* **297,** 1831
30. Taverna, S. D., Coyne, R. S., and Allis, C. D. (2002) Methylation of histone H3 at lysine 9 targets programmed DNA elimination in tetrahymena. *Cell* **110,** 701–711
31. Vastenhouw, N. L., Brunschwig, K., Okihara, K. L., Müller, F., Tijsterman, M., and Plasterk, R. H. (2006) Gene expression: long-term gene silencing by RNAi. *Nature* **442,** 882
32. Fukagawa, T., Nogami, M., Yoshikawa, M., Ikeno, M., Okazaki, T., Takami, Y., Nakayama, T., and Oshimura, M. (2004) Dicer is essential for formation of the heterochromatin structure in vertebrate cells. *Nat. Cell. Biol.* **6,** 784–791
33. Zhang, H., Alramini, H., Tran, V., and Singh, U. (2011) Nucleus-localized antisense small RNAs with 5′-polyphosphate termini regulate long term transcriptional gene silencing in *Entamoeba histolytica* G3 strain. *J. Biol. Chem.* **286,** 44467–44479
34. Zhang, H., Ehrenkaufer, G. M., Pompey, J. M., Hackney, J. A., and Singh, U. (2008) Small RNAs with 5′-polyphosphate termini associate with a Piwi-related protein and regulate gene expression in the single-celled eukaryote *Entamoeba histolytica*. *PLoS Pathogens* **4,** e1000219
35. Morf, L., Pearson, R. J., Wang, A. S., and Singh, U. (2013) Robust gene silencing mediated by antisense small RNAs in the pathogenic protist *Entamoeba histolytica*. *Nucleic Acids Res.* **41,** 9424–9437
36. Pompey, J. M., Morf, L., and Singh, U. (2014) RNAi pathway genes are resistant to small RNA mediated gene silencing in the protozoan parasite *Entamoeba histolytica*. *PloS One* **9,** e106477
37. Huguenin, M., Bracha, R., Chookajorn, T., and Mirelman, D. (2010) Epigenetic transcriptional gene silencing in *Entamoeba histolytica*: insight into histone and chromatin modifications. *Parasitology* **137,** 619–627
38. Jhingan, G. D., Panigrahi, S. K., Bhattacharya, A., and Bhattacharya, S. (2009) The nucleolus in *Entamoeba histolytica* and *Entamoeba* invadens is located at the nuclear periphery. *Mol. Biochem. Parasitol.* **167,** 72–80
39. MacFarlane, R. C., and Singh, U. (2006) Identification of differentially expressed genes in virulent and nonvirulent Entamoeba species: potential implications for amebic pathogenesis. *Infect. Immun.* **74,** 340–351
40. Diamond, L. S., Harlow, D. R., and Cunnick, C. C. (1978) A new medium for the axenic cultivation of *Entamoeba histolytica* and other *Entamoeba*. *Trans. R. Soc. Trop. Med. Hyg.* **72,** 431–432
41. Saito-Nakano, Y., Yasuda, T., Nakada-Tsukui, K., Leippe, M., and Nozaki, T. (2004) Rab5-associated vacuoles play a unique role in phagocytosis of the enteric protozoan parasite *Entamoeba histolytica*. *J. Biol. Chem.* **279,** 49497–49507
42. Födinger, M., Ortner, S., Plaimauer, B., Wiedermann, G., Scheiner, O., and Duchêne, M. (1993) Pathogenic *Entamoeba histolytica*: cDNA cloning of a histone H3 with a divergent primary structure. *Mol. Biochem. Parasitol.* **59,** 315–322
43. Liu, Y., Taverna, S. D., Muratore, T. L., Shabanowitz, J., Hunt, D. F., and Allis, C. D. (2007) RNAi-dependent H3K27 methylation is required for heterochromatin formation and DNA elimination in Tetrahymena. *Genes Dev.* **21,** 1530–1545
44. Rosenfeld, J. A., Wang, Z., Schones, D. E., Zhao, K., DeSalle, R., and Zhang, M. Q. (2009) Determination of enriched histone modifications in non-genic portions of the human genome. *BMC Genomics* **10,** 143
45. Kosar, M., Bartkova, J., Hubackova, S., Hodny, Z., Lukas, J., and Bartek, J. (2011) Senescence-associated heterochromatin foci are dispensable for cellular senescence, occur in a cell type- and insult-dependent manner and follow expression of p16(ink4a). *Cell Cycle* **10,** 457–468
46. Papazyan, R., Voronina, E., Chapman, J. R., Luperchio, T. R., Gilbert, T. M., Meier, E., Mackintosh, S. G., Shabanowitz, J., Tackett, A. J., Reddy, K. L., Coyne, R. S., Hunt, D. F., Liu, Y., and Taverna, S. D. (2014) Methylation of histone H3K23 blocks DNA damage in pericentric heterochromatin during meiosis. *eLife* **3,** e02996
47. Pearson, R. J., Morf, L., and Singh, U. (2013) Regulation of H2O2 stress-responsive genes through a novel transcription factor in the protozoan pathogen *Entamoeba histolytica*. *J. Biol. Chem.* **288,** 4462–4474
48. Ellison, T. J., and Kedes, D. H. (2014) Variable episomal silencing of a recombinant herpesvirus renders its encoded GFP an unreliable marker of infection in primary cells. *PloS One* **9,** e111502
49. Lund, A. H., and van Lohuizen, M. (2004) Polycomb complexes and silencing mechanisms. *Curr. Opin. Cell Biol.* **16,** 239–246
50. Moazed, D., Bühler, M., Buker, S. M., Colmenares, S. U., Gerace, E. L.,

Gerber, S. A., Hong, E. J., Motamedi, M. R., Verdel, A., Villén, J., and Gygi, S. P. (2006) Studies on the mechanism of RNAi-dependent heterochromatin assembly. *Cold Spring Harbor Symp. Quant. Biol.* **71,** 461–471
51. Pokholok, D. K., Hannett, N. M., and Young, R. A. (2002) Exchange of RNA polymerase II initiation and elongation factors during gene expression *in vivo*. *Mol. Cell* **9,** 799–809
52. Gao, L., and Gross, D. S. (2008) Sir2 silences gene transcription by targeting the transition between RNA polymerase II initiation and elongation. *Mol. Cell. Biol.* **28,** 3979–3994
53. Johnson, A., Wu, R., Peetz, M., Gygi, S. P., and Moazed, D. (2013) Heterochromatic gene silencing by activator interference and a transcription elongation barrier. *J. Biol. Chem.* **288,** 28771–28782
54. Hemming, S. A., Jansma, D. B., Macgregor, P. F., Goryachev, A., Friesen, J. D., and Edwards, A. M. (2000) RNA polymerase II subunit Rpb9 regulates transcription elongation *in vivo*. *J. Biol. Chem.* **275,** 35506–35511
55. Tovy, A., and Ankri, S. (2010) Epigenetics in the unicellular parasite *Entamoeba histolytica*. *Future Microbiol.* **5,** 1875–1884
56. Chen, E. S., Zhang, K., Nicolas, E., Cam, H. P., Zofall, M., and Grewal, S. I. (2008) Cell cycle control of centromeric repeat transcription and heterochromatin assembly. *Nature* **451,** 734–737
57. Neumann, P., Yan, H., and Jiang, J. (2007) The centromeric retrotransposons of rice are transcribed and differentially processed by RNA interference. *Genetics* **176,** 749–761
58. Weinberg, M. S., Villeneuve, L. M., Ehsani, A., Amarzguioui, M., Aagaard, L., Chen, Z. X., Riggs, A. D., Rossi, J. J., and Morris, K. V. (2006) The antisense strand of small interfering RNAs directs histone methylation and transcriptional gene silencing in human cells. *RNA* **12,** 256–262
59. Eichten, S. R., Ellis, N. A., Makarevitch, I., Yeh, C. T., Gent, J. I., Guo, L., McGinnis, K. M., Zhang, X., Schnable, P. S., Vaughn, M. W., Dawe, R. K., and Springer, N. M. (2012) Spreading of heterochromatin is limited to specific families of maize retrotransposons. *PLoS Genet.* **8,** e1003127
60. Wang, J., Reddy, B. D., and Jia, S. (2015) Rapid epigenetic adaptation to uncontrolled heterochromatin spreading. *eLife* **4,** 10.7554/eLife.06179
61. Wang, J., Lawry, S. T., Cohen, A. L., and Jia, S. (2014) Chromosome boundary elements and regulation of heterochromatin spreading. *Cell. Mol. Life Sci.* **71,** 4841–4852
62. Deshpande, G., Calhoun, G., and Schedl, P. (2005) Drosophila argonaute-2 is required early in embryogenesis for the assembly of centric/centromeric heterochromatin, nuclear division, nuclear migration, and germ-cell formation. *Genes Dev.* **19,** 1680–1685
63. Cam, H. P., Sugiyama, T., Chen, E. S., Chen, X., FitzGerald, P. C., and Grewal, S. I. (2005) Comprehensive analysis of heterochromatin- and RNAi-mediated epigenetic control of the fission yeast genome. *Nat. Genet.* **37,** 809–819
64. Hall, I. M., Shankaranarayana, G. D., Noma, K., Ayoub, N., Cohen, A., and Grewal, S. I. (2002) Establishment and maintenance of a heterochromatin domain. *Science* **297,** 2232–2237
65. Kim, D. H., Villeneuve, L. M., Morris, K. V., and Rossi, J. J. (2006) Argonaute-1 directs siRNA-mediated transcriptional gene silencing in human cells. *Nat. Struct. Mol. Biol.* **13,** 793–797
66. Morris, K. V., Chan, S. W., Jacobsen, S. E., and Looney, D. J. (2004) Small interfering RNA-induced transcriptional gene silencing in human cells. *Science* **305,** 1289–1292
67. Ayoub, N., Noma, K., Isaac, S., Kahan, T., Grewal, S. I., and Cohen, A. (2003) A novel jmjC domain protein modulates heterochromatization in fission yeast. *Mol. Cell. Biol.* **23,** 4356–4370
68. Saze, H., Shiraishi, A., Miura, A., and Kakutani, T. (2008) Control of genic DNA methylation by a jmjC domain-containing protein in *Arabidopsis thaliana*. *Science* **319,** 462–465
69. Janowski, B. A., Huffman, K. E., Schwartz, J. C., Ram, R., Nordsell, R., Shames, D. S., Minna, J. D., and Corey, D. R. (2006) Involvement of AGO1 and AGO2 in mammalian transcriptional silencing. *Nat. Struct. Mol. Biol.* **13,** 787–792
70. Wang, J., Czech, B., Crunk, A., Wallace, A., Mitreva, M., Hannon, G. J., and Davis, R. E. (2011) Deep small RNA sequencing from the nematode Ascaris reveals conservation, functional diversification, and novel developmental profiles. *Genome Res.* **21,** 1462–1477
71. Horwich, M. D., Li, C., Matranga, C., Vagin, V., Farley, G., Wang, P., and Zamore, P. D. (2007) The *Drosophila* RNA methyltransferase, DmHen1, modifies germline piRNAs and single-stranded siRNAs in RISC. *Curr. Biol.* **17,** 1265–1272
72. Talbert, P. B., and Henikoff, S. (2006) Spreading of silent chromatin: inaction at a distance. *Nat. Rev. Genet.* **7,** 793–803